Relationship Between Molecular Structure and Surface Properties of Self-Assembled Monolayers

Huimin Li

Dissertation submitted to the faculty of the Virginia Polytechnic Institute and State University in partial fulfillment of the requirements for the degree of

Doctor of Philosophy
in
Chemistry

Mark R. Anderson, Chair
Karen Brewer
Gary L. Long
John R. Morris
Rickey M. Davis

September 8, 2004
Blacksburg, Virginia

Keywords: Adhesion Promoter, Corrosion Protection, RAIRS, EIS, Structure Property Relationship, Self-Assembled Monolayer

Relationship Between Molecular Structure and Surface Properties of Self-Assembled Monolayers

Huimin Li

(Abstract)

Polyimides are frequently used as insulating layers in the microelectronics industry. These polymers are tough, have high thermal stability, and have favorable dielectric properties; consequently, polyimides are excellent materials for insulating layers in microelectronic devices. In this research, self-assembled monolayers are investigated for use as an adhesion promoter for metal substrates, and for corrosion protectors of the metal surface.

Gold substrates modified by adsorption of 3- and 4-aminothiophenol monolayers, 3- and (4-mercaptophenyl) phthalimide (MPP) monolayers, and by reaction of the 3- and 4-aminothiophenol monolayers with the phthalic anhydride were studied using reflection absorption infrared spectroscopy, contact angle measurement, ellipsometry, and electrochemical measurements. Reactions on the monolayers are used to model the attachment of an insulating polyimide to the substrate. The covalent attachment of the anhydride is confirmed, and the efficiency of the reaction of the aminothiolphenol monolayers is investigated. The reactivity of the aminothiolphenol monolayers is found to depend on the position of the amino-group around the phenyl ring.

Impedance spectroscopy is used to investigate the ionic insulating properties of these systems. The 4-mercaptophthalimide monolayer is found to have the highest monolayer resistance to ion transport. This result suggests that it forms the most densely packed monolayer. The monolayer resistance of the surfaces prepared by adsorption of the aminothiolphenol isomers followed by reaction with phthalic anhydride is much lower than the corresponding deposited mercaptophthalimide monolayers. These results suggest that the reaction efficiency is low. Impedance spectroscopy and polarization measurements suggests a higher protection efficiency for 3-mercaptophenylphthalimide. These results will be discussed in the context of the ability of the isomeric mercaptophthalimide monolayers to serve as protectors against substrate corrosion.

Acknowledgements

I would like to acknowledge my advisor, Dr. Mark R. Anderson for his guidance, support, appreciation, and encouragement for my research work at Virginia Tech during past five years. As an educator, he tried to raise his students as independent researchers and scientists. He has been tremendous help in my dissertation writing and presentation.

I gratefully thank Dr. Karen Brewer, Dr. John Morris, Dr. Gary Long and Dr. Richey Davis for their valuable contributions as members of my advisory committee.

Many thanks go to the fellow students in Professor Anderson's group. When I first joined the group, Professor Anderson was on his one-year vacation. Dr. Charles D. Taylor, a former group member, helped me to start up. I also thank Dr. Francisco T. Cavadas, Alice Harper, Stephanie Hooper for helping me improve my presentation skills.

I am also thankfur to my friends in the chemistry department for their friendship, refreshing talk, and sharing of their devices and chemicals.

I dearly thank my parents who brought me up and encouraged my pursuit of higher knowledge. I owe everything to my husband and my son for their love and unconditional support, without which this would not have been possible.

Table of Contents

Table of Figures

Table of Schemes

Table of Equations

List of Tables

Chapter 1

Overview and Significance of Research

The perceived relevance of self-assembled monolayers to science and technology initiated the interest in the general area of self-assembled monolayers. Self-assembled monolayers (SAMs) have become the focus of intensive investigation because they provide a facile means of defining the chemical composition and structure of a surface. Self-assembled monolayers have potential applications in corrosion prevention, lubrication, adhesion, and more because of their dense and stable structure. Understanding the fundamental relationships between molecular structure and monolayer interfacial properties is essential to the applications of self-assembled monolayers.

In this research, four SAMs composed of aromatic thiols with different functional tail groups and different substitution patterns were investigated to address the relationship between the molecular structure and the surface properties of SAMs. The goal is to understand how the molecular structure at microscopic level affects the physical properties of interface at macroscopic level. Orientation of monolayers on the surface, surface energy, thickness of monolayers, surface coverage, and reductive desorption peak potential of SAMs give us a picture of the SAMs and help to explain the ionic insulating properties of SAMs. The monolayers with active tail groups also provide a foundation for attachment of additional molecular layers to the surface. The surface reaction of monolayers is studied as the model system of adhesion of polyimide onto gold substrate.

The reactivity is investigated by studying the surface properties of mixed SAMs. The literature relevant to the general properties of SAMs and object of this thesis is reviewed.

1.1 Self-assembled Monolayers (SAMs) Literature Review

1.1.1 Concept of Self-assembled Monolayers

In a general sense, self-assembled monolayers can be defined as well-ordered and oriented organic molecular films formed spontaneously upon the immersion of a substrate into a solution containing an active surfactant molecule in an organic solvent (figure 1). The respective molecules consist of three units: a surface-active head group which binds strongly to the substrate, a specific functional tail group that constitutes the outer surface of the film and modifies bulk surface properties, and a chain or backbone that connects the head and tail groups. It is well known that the lateral density and structure of self-assembled monolayers are the result of a delicate interplay between the substrate-adsorbate interactions, the nonbonded interactions between adsorbates – electrostatic and Van der Waals forces, – and the intramolecular interactions such as bond stretches, angle bends, and torsions. Tail groups can also affect the self-assembled monolayers' structure significantly, providing it has a strong polar characteristic or is sufficiently large. The process to prepare self-assembled monolayers is simple and only minimum amounts of organic molecules are needed. The flexiblility to design self-assembled monolayers with various functional tail groups to accomplish desired surface properties and to possibly control the structure in the nanometer regime is an attractive feature of self-assembled monolayers. These features created significant research activity

in the area of self-assembled monolayers, and progress in the understanding of these self-assembled monolayers on a microscopic level has advanced significantly since the 1980s.

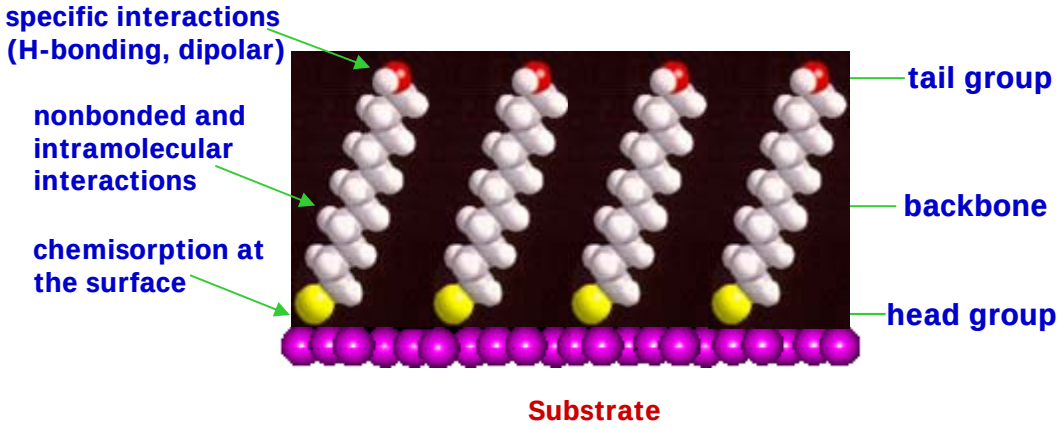

Figure 1.1. Schematic of self-assembled monolayers, including the constituents of a molecue and the driving force for the spontaneous formation of self-assembled monolayers.

1.1.2 Structure of various self-assembling systems

Self-assembling systems are classified by the "pair" of the chemisorbing head group of the organic molecule and the substrate. Many systems have been used to form self-assembled monolayers. Figure 1.2 shows some molecules that are frequently-used for self-assembled monolayers: *n*-alkanethiols[1,2,3,4,5,6,7,8,9,10,11,12,13,14,15], α, ω-alkanedithiol, ω-mercaptoalkanol, ω-mercaptoalkane carboxylic acid, oligophenylthiols, 1, 1′-dialkyl-disulfide, and alkyltrichlorosilane. Substrates used to support self-assembled monolayers include gold, silver, copper, iron, semiconductors such as GaAs(100), InP(100), liquid mercury, and hydroxylated surfaces such as oxidized silicon or mica. Alkanethiols adsorbed on Au(1 1 1) are probably the most common system studied.

Organosilicon monolayers on hydroxylated surfaces have also been extensively studied. This review will focus on thiols on gold and copper.

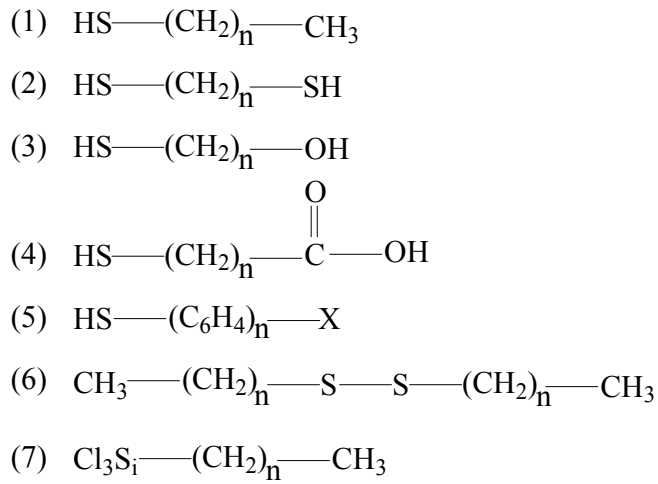

Figure 1.2. Some frequently used molecules for self-assembled monolayers. (1) *n*-alkanethiols; (2) α, ω-alkanedithiol; (3) ω-mercaptoalkanol; (4) ω-mercaptoalkane carboxylic acid; (5) oligophenylthiols; (6) 1, 1′-dialkyl-disulfide; (7) alkyltrichlorosilane.

Several research groups investigated the orientation of alkanethiols at Au substrates. Ulman and co-workers[16] calculated the free energies of various orientations of long-chain alkanethiols using computer modeling. They predicted a molecular tilt of the carbon backbone of about 30° from normal and a rotation about the chain axis of about 55° from the minima in free energy of the systems based on van der Waals interactions between adjacent molecules at single crystals of Au. From infrared spectral data interpreted on the basis of surface selection rules, a tilt angle of about 40° from the surface normal for long-chain alkanethiols at Au with a rotation about the chain axis of 50° has been estimated by Nuzzo and co-workers[17]. Bryant and Pemberton studied Raman scattering in the ν(C-S), ν(C-C), ν(S-H), and ν(C-H) region of a series of 1-alkanethiol films at Au and qualitatively deduced an orientation of alkanethiols at Au

with use of surface selection rules which have been described by Moskovits[18] for rough surfaces. The fundamental basis of these selection rules is as follows. The coordinate frame of a surface is defined in such a way that the *z* axis is perpendicular to the surface and the *x* and *y* axes are parallel to the surface. With excitation to the red of the surface plasmon wavelength, vibrations of surface-confined molecules with *zz* tensor components will be enhanced to a larger extent than vibrations with *xz* or *yz* components. Stretching vibrations were used for interpretation of orientation in their alkanethiol systems because they were assumed to have a large contribution from the tensor component along the axis of the vibration. Their results agree with previous determinations of orientation on Au.

Most of the initial investigations on self-assembled monolayers focus on the adsorption of linear alkanethiols onto gold surfaces. While this system is one of the most thoroughly studied, self-assembled monolayers of aromatic thiols have also attracted attention recently because of the gauche defects that can be introduced into linear alkanethiols resulting in surface disorder[19]. Therefore, a preferred system will be one in which conformational disorder has been eliminated. This is achieved using rigid molecules where surface functional groups have no conformational freedom and are "stuck" at the surface. Aromatic thiols have the required rigidity. While the usefulness of using rigid thiols for SAM formation has been demonstrated, the synthetic difficulties and poor solubility associated with multi-ring aromatic thiols impede the widespread study of aromatic thiols[20].

Liao and co-workers studied the adsorption kinetics of five rigid 4-mercaptobiphenyls onto a polycrystalline gold surface using the quartz crystal microbalance (QCM) technique[20]. They provided the first experimental evidence of the

influence of the molecular dipole and the electron density on the S-atom on the adsorption process of aromatic thiols on gold. Like *n*-alkanethiols, the aromatic thiol SAM formation process can also be described as a two-step mechanism: first, a fast adsorption step followed by a much slower orientational ordering step. The mass equilibrium was found to be reached within the first minute for *n*-alkanethiols [21,22,23], and the first few minutes for aromatic thiols[20]. The first step was suggested to be described by the following equation:

$$\text{X-Ph-Ph-SH (sol)} \rightleftharpoons \text{X-Ph-Ph-SH}\bullet\ \text{Au}_n \rightleftharpoons \text{X-Ph-Ph-S}^{-}\text{Au}^{+}\bullet\text{Au}_n + 1/2\ \text{H}_2 \quad (1.1)$$

The chemical bond between the thiolate and gold is stronger for 4-mercaptobiphenyl than that for alkanethiol due to the bigger chemisorption potential values than alkanthiols[21].

A new chemisorption model that takes the interaction between adsorbing molecules into account was developed by Liao and co-workers to fit the adsorption kinetics of 4-mercaptobiphenyl molecules. The Langmuir isotherm model assumes that there is no interaction between adsorbates. The Langmuir isotherm fits the adsorption kinetics of *n*-alkanethiols on gold successfully[21], but does not fit well with aromatic thiols. This observation has also been reported with other aromatic thiols[24]. The interaction parameter values from the fit of their chemisorption model indicated a repulsive interaction between aromatic thiol molecules, which dominates over attractive van der Waals forces when molecule has big dipole moment and slows down both the adsorption and desorption process.

Whelan *et al.* studied benzenethiol self-assembled monolayers on Au (1 1 1)[25]. In the high-resolution electron energy loss spectroscopy, the S-H stretching vibration is absent and the aromatic vibrational bands are present. They both suggest lose of the

sulfhydryl hydrogen during adsorption. XPS spectroscopy of the sulfur(2p) and carbon(1s) core levels supported the chemisorbed benzenethiolate as the primary adsorbate species. The intensity of the out-of-plane C-H deformation is smaller than that of the C-H stretching vibration in the high-resolution electron energy loss spectroscopy spectrum. The film thickness estimated by attenuation of the Au($4f_{7/2}$) signal upon self-assembly was 6.0-8.3 Å. The sulfur coverage was determined to be 0.45 monolayers in their study. All these results supported a adsorption geometry with a phenyl ring oriented normal to the Au surface.

One of the interesting aspects of aromatic thiol adsorption is that the phenyl ring allows substitution in *ortho, meta, and para* positions. The effect of isomeric structure on the organization and electrochemistry of the SAMs of the three isomers of aminothiophenol, ATP (I-III) (shown in Scheme 1), were reported by Batz *et al.*[24]. In their studies, all ATP SAMs were prepared in an aqueous solution of 0.1 M sulfuric acid. Due to their different intermolecular and surface interactions, the SAMs of the three isomers are organized differently. The packing density was 4-ATP>3-ATP>2-ATP, and the reductive desorption potentials were ambiguous. They also found that the different isomers are likely to orient perpendicular to the surface. While the amino group of the 4-ATP points away from the substrate, that of the 2-ATP is located close to the gold surface so 2-ATP probably interacts with the gold surface with both the amine and the mercapto groups. The different position and orientation of the amine group relative to the substrate and the SAM/electrolyte interface resulted in the different interfacial properties, such as capacity, copper deposition, palladium (II) extraction, of three isomers. Moreover, these isomeric SAMs can be easily oxidized but yield different surface products. The

difference in the chemical reactivity can also be attributed to the difference in the extent of interaction of the amino group with the solution as well as with the adjacent molecules.

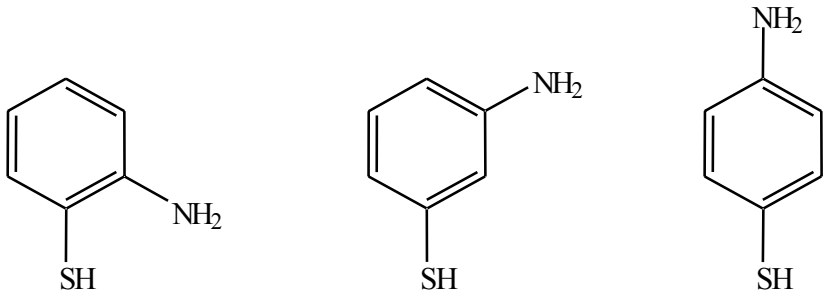

2-ATP 3-ATP 4-ATP

Scheme 1.1. Structure of three isomers of aminothiophenol (ATP)

1.1.3 Self-assembled Monolayers as corrosion inhibitors

Modifying the reactive metal surface by organic molecules or polymers can reduce the corrosion rate of metals significantly. Traditionally, organic coating which are applied as thick multilayer films with thickness ranging from some 10 μm to some 100 μm are used to protect many reactive materials from corrosion. However, thin and ultrathin corrosion protecting films are of considerable interest especially in modern areas of materials research such as microelectronic devices or micromechanics. The thickness of any thin and ultrathin corrosion protecting film must be much less than 0.1 μm. Self-assembled monolayers with thicknesses less than 10 nm are particularly attractive for these applications. Many organic coatings can impede the penetration of water and oxygen to the metal/polymer interface, and this barrier property of the coating has long

been believed to give rise to the corrosion stability[26]; however, many other organic coatings are highly permeable for water and oxygen. It is believed, therefore, that in this case the corrosion protection is due to some specific electrochemical properties of metal/polymer interface, in particular the formation of an extended diffuse double layer, but not the barrier effect on the diffusion process[27,28]. There are two partial reactions of the corrosion process, the anodic metal dissolution and the cathodic oxygen reduction. Corrosion inhibitors reduce the rate of either or both of these. In the presence of defects (pores, pinholes, etc.), very aggressive species, such as OH· and OH^-, liberated during the electrochemical reduction of oxygen will immediately attack and destroy chemical bonds within the coatings[29,30]. Therefore, the composition, structure, and chemical bonds of the metal/coating interface are more vital than the thickness of the coating in the corrosion inhibition. Thus, improving the chemical interaction between the first monolayer of the coating and the substrate will inhibit electrochemical reactions such as the reduction of oxygen on the metal/coating interface and the bonds may withstand the attack of water and other aggressive species (OH·, OH^-).

It is well known that many organic molecules are used as corrosion inhibitors[31,32] and molecular self-assembly is one of the surface modification techniques that meet the requirements for the corrosion protection. Alkanethiol self-assembled monolayers have proven to be excellent inhibitors of oxygen reduction and are not easily destroyed by the radicals set free during the oxygen reduction[33]. Self-assembled monolayers act as an interface inhibitor from a mechanistic point of view. The monomolecular adsorption layers can prevent the dissolution of the substrate and the reduction of oxygen by changing the potential drop across the interface and/or the reaction mechanism.

The corrosion resistance of a *n*-alkanethiol monolayer modified copper surface was first investigated by Laibinis and Whitesides in atmosphere under ambient conditions [34]. Several groups, such as Scherer et al. [35], Feng *et al.*[36], Laibinis[37,38], and Itoh *et al.*[39,40,41,42], investigated the performance of different alkanethiolate SAMs as protective coatings on copper in aggressive electrolytes. These alkanethiolate SAMs were reported to be able to provide a diffusional barrier against the transport of O_2[34,42], H_2O[37], and aqueous ions[38]. Detailed, molecular-level investigations of the effect of various structural parameters of SAMs, such as thickness, packing density, crystallinity, and composition on the level of protection against corrosion of the copper substrate revealed that longer-chain thiols form thicker SAMs with a higher level of dense packing and crystallinity within the hydrocarbon layer offered greater protection on the copper surface[34,38]. Due to the difficulties in synthesis of long chain *n*-alkanethiols, long-chain *ω*-alkoxy-*n*-alkanethiols were synthesized to form SAMs with greater thickness (40-60 Å)[43]. Both the chain length of the adsorbate and the position of the ethereal unit along the hydrocarbon chain affected the performances of these SAMs as barrier layers.

Ultrathin protective films of two-dimensional polymers prepared by modifying an alkanethiol self-assembled monolayer adsorbed on copper have also been studied. Normally, bifunctional organic molecules with the head group ready to undergo further hydrolysis are used to form self-assembled monolayers on copper. Aramaki group has been working on corrosion protection of copper by modification of 11-mercapto-1-undecanol (MUO) self-assembled monolayer with different modifiers and different procedures for several years[44,45,46,47,48]. They optimized modifiers to eliminate the contamination of Cl^- and simplified the procedures in the film preparation from multistep

modification to single-step modification. The corrosion protection of copper was increased markedly from fairly protected to significantly high, over 90%. Mekhalif et al. first reported the formation of a well-organized (3-mercaptopropyl)trimethoxysilane (MPTS) SAMs on copper surfaces[49]. A thin siloxane network relatively free from defects was formed after hydrolysis of the methoxy head groups. 3(heptafluoroisopropoxy)propyltrichlorosilane (HIPS) was subsequently attached onto the MPTS-modified copper surface following hydrolysis. The corrosion-inhibitive properties of film at each stage were characterized by calculating a blocking factor (BF) from cyclic voltammetry measurements. The blocking factor of MPTS SAMs increased remarkably from 50% to 84% with the HIPS attachment. Their work demonstrated that the two-dimensional film dramatically improved the protection of the underlying copper substrate with only a modest increase in the thickness of the SAMs.

In most studies of corrosion protection properties by SAMs on copper, organic solvents such as ethanol, isooctane, and hexane were used during the preparation of the SAMs because of the limited solubility of organic molecules consisted the SAMs. Water, however, is a ubiquitously used solvent for many applications involving copper, particularly in chemical process industries. Another advantage of water is that it does not have problems of waste disposal encountered when using organic solvents. SAMs prepared by adsorption of sodium *S*-alkyl thiosulfates ($CH_3(CH_2)_{n-1}S_2O_3^-Na^+$) (C*n*TS) onto copper from aqueous solution were investigated as an alternative to alkanethiol adsorption[50]. Compared to alkanethiols, the solubility of these ionic compounds in water is greatly improved due to the presence of an ionic headgroup. These results revealed that, although the thiosulfate SAMs formed in water have a more disordered structure with a

greater number of defects and a lower surface coverage compared to alkanethiol SAMs and thiosulfate SAMs formed in ethanol and THF, they do have resistances that were 2-3 orders greater than that for the uncoated copper when the chain length was long (n = 12, 14). A comparison of $C_{14}TS$ to benzotriazole showed potential application of longer-chained thiosulfates in inhibiting the corrosion of copper in aqueous environments.

Only a few studies about SAMs consisted of aromatic molecules as protection films against copper corrosion have been reported compared with a number of studies of alkanethiol SAMs. Hackerman and Khaled studied the inhibiting properties of a series of *ortho*-substituted anilines for copper corrosion[51]. These compounds all showed inhibiting properties for copper corrosion in HCl solutions to some extent. The inhibiting efficiency was affected by the molecular structure of *o*-substituted aniline and was found to increase in the following order, $-C_2H_5 > -Cl > -F > -CH_3 > -OCH_3 > -OC_2H_5$.

1.1.4 Reactions on Self-assembled Monolayer Modified Gold Substrate

The characterization of products bound to the solid supports is more difficult than that of products of organic synthesis in solution. There are some disadvantages of self-assembled monolayers on smooth, reflective surface. First, some rapid, sensitive techniques such as NMR spectroscopy, mass spectrometry, elemental analysis, and X-ray spectroscopy which are commonly used to analyze the products of organic synthesis in solution are useless when working with reactions on monolayers. Second, the extremely small quantities involved make many analytical tools useless. Finally, a combination of techniques are often required to characterize the products on the surface and the problem of estimating the yield becomes quite significant. One of the advantages is that reactions

on monolayers can be studied by a wide range of techniques used in characterization of self-assembled monolayer including reflection absorption infrared spectroscopy, contact angle measurements, X-ray photoelectron spectroscopy, surface plasmon resonance, atomic force microscopy, ellipsometry, quartz crystal microbalance, electrochemical methods.

1.2 Thesis Statement

It is concluded from the studies reported previously that structure of molecules that compose the self-assembled monolayers affects surface properties of SAMs interfaces. Interestingly, the effect of isomeric structure of aromatic thiols has rarely been reported. Research presented in this thesis studies the properties of aromatic thiols self-assembled monolayers for use as an adhesion promoter and as corrosion protectors of metal surfaces. SAMs prepared with aminothiolphenol on modified gold surfaces are reacted with phthalic anhydride (PA) to serve as a polyimide model system for studying polyimides adhesion. Two isomers of ATP, 3-ATP and 4-ATP, were investigated as coupling agents for polyimide adsorption on metals to address the effect of substitution patterns on the interfacial reactivity. Electrochemical impedance spectroscopy (EIS) and polarization measurements were used to investigate the corrosion protection efficiency of these SAMs on metal surfaces. The passivation properties of ATP monolayers, mercaptophenylthalimide (MPP) monolayers (two isomers in each case, all prepared by deposition from thiol solution) and monolayers prepared by reaction of the aminothiophenol with the anhydride on gold substrates were investigated using EIS. This thesis research has two objectives.

- First is to study the influence of functional tail groups with different hydrophobility and substitution patterns on the ionic insulating properties of SAMs.
- Second is to compare the ionic insulating properties of self-assembled monolayers prepared by deposition from solution and by reactions of the monolayers to see if a surface with good ionic insulating properties can be prepared through reactions of the monolayer.

Two isomers of MPP SAMs, 3-MPP and 4-MPP, were also investigated to protect copper corrosion. Again, the relationship between molecular structure and the corrosion protection efficiency is our interest.

1.3 References

1. Nuzzo, R.G.; Dubois, L.H.; Allara, D.L. *J. Am. Chem. Soc.* **1990,** *112,* 558

2. Nuzzo, R.G.; Korenic, E.M.; Dubois, L.H. *J. Chem. Phys.* **1990,** *93,* 767

3. Camillone, N.; Chidsey, C.E.D.; Liu, G.-Y.; Scoles, G. *J. Chem. Phys.* **1993,** *98,* 4234

4. Fenter, P.; Eisenberger, P.; Liang, K.S. *Phys. Rev. Lett.* **1993,** *70,* 2447

5. Poirier, G.E.; Tarlov, M.J. *Langmuir* **1994,** *10,* 2853

6. Delamarche, E.; Michel, B.; Gerber, C.; Anselmetti, D.; Güntherodt, H.-J.; Wolf, H.; Ringsdorf, H. *Langmuir* **1994,** *10,* 2869

7. Bucher, J.P.; Santesson, L.; Kern, K. *Appl. Phys. A* **1994,** *59,* 135

8. Parikh, A.N.; Allare, D.L. *J. Chem. Phys.* **1992,** *96,* 927

9. Bryant, M.A.; Pemberton, J.E. *J. Am. Chem. Soc.* **1991,** *113,* 8284

10. Dubois, L.H.; Nuzzo, R.G. Ann. Rev. Phys. Chem. 1992, 43, 437

11. Anselmetti, D.; Baratoff, A.; Güntherodt, H.-J.; Delamarche, E.; Michel, B.; Gerber, C.; Kang, H.; Wolf, H.; Ringsdorf, H. *Europhys. Lett.* **1994,** *27,* 365

12. Delamarche, E.; Michel, B.; Biebuyck, H.A.; Gerber, C. *Adv. Mater.* **1996,** *8,* 719

13. Yeganeh, M.S.; Dougal, S.M.; Polizzotti, R.S.; Rabinowitz, P. *Phys. Rev. Lett.* **1995,** *74,* 1811

14. Fenter, P.; Schreiber, F.; Berman, L.; Scoles, G.; Eisenberger, P.; Bedzyk, M. *Surf. Sci.* **1998,** *412/413,* 213

15. Fenter, P.; Schreiber, F.; Berman, L.; Scoles, G.; Eisenberger, P.; Bedzyk, M. *Surf. Sci.* **1999,** *425,* 138

16. Ulman, A.; Eilers, J.G.; Tilman, N. *Langmuir* **1989,** *5,* 1147

17. Nuzzo, R.G.; Dubois, L.H.; Allara, D.L. *J. Am. Chem. Soc.* **1990,** *112,* 558

18. Moskovits, M. *Rev. Mod. Phys.* **1985,** *57,* 783

19. Whitesides, G. M.; Laibinis, P.E. *Langmuir* **1990,** *6,* 87

20. Liao, S.; Shnidman, Y.; Ulman, A. *J. Am. Chem. Soc.* **2000,** *122,* 3688

21. Karpovidh, D. S.; Blanchard, G. J. *Langmuir* **1994,** *10,* 3315

22. Buck, M.; Grunze, M.; Eiser, F.; Fiser, J.; Trger, F. J. *Vac. Sci. Technol., A* **1992,** *10,* 926

23. Hähner, G.; Wll, Ch.; Buck, M.; Grunze, M. *Langmuir* **1993,** *9,* 1955

24. Batz, V.; Schneeweiss, M. A.; Kramer, D.; Hagenström, H.; Kolb, D. M.; Mandler, D. *Journal of Electroanalytical Chemistry* **2000,** *491,* 55

25. Whelan, C.M.; Smyth, M.R.; Barnes, C.J. *Langmuir* **1999,** *15,* 116-126

26. Kinloch, A. J. *Adhesion* **1979,** *3*

27. Feser, R.; Stratmann, M. *Werkst. Korros.* **1991,** *42,* 187

28. Stratmann, M.; Feser, R.; Leng, A. *Electrochim. Acta* **1994,** *39,* 1207

29. Hammond, J. S.; Holubka, J. W.; Dickie, R. A. *J. Coat. Technol.* **1979,** *51,* 45

30. Leidheiser, H., Jr. ed., *Corrosion Control by Organic Coatings,* NACE, Houston, **1981**

31. Brasher, D. M.; Mercer, A. D. *Br. Corros, J.* **1967,** *95,* 122

32. Schmitt, G. *Br. Corros. J.* **1984,** *9,* 165

33. Vago, E.; Weldige, K. de; Rohwerder, M.; Stratmann, M. *Fresen. J. Anal. Chem*. **1995,** *335,* 316

34. Laibinis, P. E.; Whitesides, G. M. *J. Am. Chem. Soc.* **1992,** *114,* 9022

35. Scherer, J.; Vogt, M. R.; Magnussen, O. M.; Behm, R. J. *Langmuir* **1997,** *13,* 7045

36. Feng, Y. Q.; Teo, W. K.; Siow, K. S.; Gao, Z. Q.; Tan, K. L.; Hsieh, A. K. *J. Electrochem. Soc.* **1997,** *144,* 55

37. Jennings, G. K.; Laibinis, P. E. *Colloids Surf., A* **1996,** *116,* 105

38. Jennings, G. K.; Munro, J. C.; Yong, T. –H.; Laibinis, P. E. *Langmuir* **1998,** *14,* 6130

39. Itoh, M.; Nishihara, H.; Aramaki, K. *J. Electrochem. Soc.* **1994,** *141,* 2018

40. Itoh, M.; Nishihara, H.; Aramaki, K. *J. Electrochem. Soc.* **1995,** *142,* 1839

41. Itoh, M. Nishihara, H.; Aramaki, K. *J. Electrochem. Soc.* **1995,** *142,* 3696

42. Ishibashi, M.; Itoh, M.; Nishihara, H.; Aramaki, K. *Electrochim. Acta* **1996,** *41,* 241

43. Jennings, G. K.; Yong, T.-H.; Munro, J. C.; Laibinis, P. E. *J. Am. Chem. Soc.* **2003,** *125,* 2950

44. Yamamoto, Y.; Nishihara, H.; Aramaki, K. *J. Electrochem. Soc.* **1993,** *140,* 436

45. Itoh, M.; Nishihara, H.; Aramaki, K. *J. Electrochem. Soc.* **1994,** *141,* 2018

[46]. Haneda, R.; Nishihara, H.; Aramaki, K. *J. Electrochem. Soc.* **1997,** *144,* 1215

47. Haneda, R.; Nishihara, H.; Aramaki, K. *J. Electrochem. Soc.* **1998,** *145,* 1856

48. Haneda, R.; Aramaki, K. *J. Electrochem. Soc.* **1998,** *146,* 2786

49. Sinapi, F.; Delhalle, J.; Mekhalif, Z. *Materials Science and Engineering C* **2002,** *22,* 345

50. Lusk, A. T.; Jennings, G. K. *Langmuir* **2001,** *17,* 7830

51. Khaled, K. F.; Hackerman, N. *Electrochimica Acta* **2004,** *49,* 485

Chapter 2

Instrumentation and Experimental Procedures

2.1 Reflection-absorption Infrared Spectroscopy

Reflection-absorption infrared spectroscopy (RAIRS) was used to characterize the orientation of the molecules within the surface monolayers. Reflection-absorption infrared spectra were obtained using a Nicolet model 710 FTIR equipped with a Spectra-Tech model FT-80 fixed grazing angle specular reflectance sample apparatus at an incident angle of 80° (see figure 2.1) and an HgCdTe detector which was cooled by liquid nitrogen. A Cambridge Physical Sciences IR polarizer (IGP228) was used to polarize the infrared source light normal to the substrate surface (P polarizer). All spectra were collected at a resolution of 2 cm^{-1} using 1024 interferometer scans. All spectra presented here are difference spectra obtained by subtracting spectra of bare gold substrate from spectra of modified substrates.

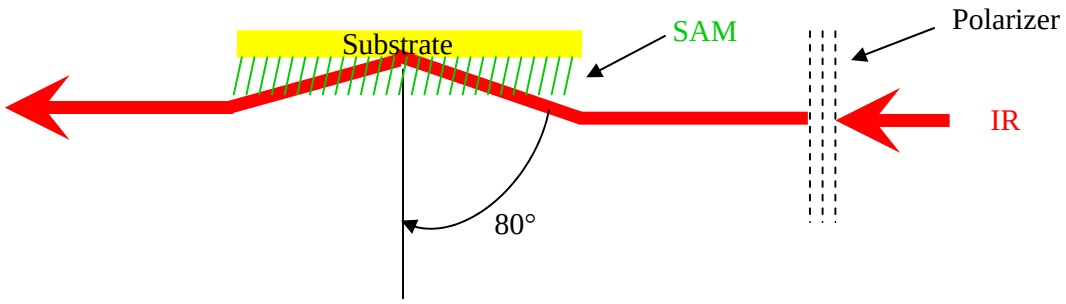

Figure 2.1. Schematic of reflection assembly used in RAIRS. A substrate is placed on top of a reflection attachment with the sample side down. The IR light is directed to the sample surface by the reflection attachment and then reflected back to the attachment by the substrate. The reflection attachment then reflects the light to the detector.

2.2 Electrochemical Measurements

All electrochemistry experiments were performed using either a CH Instruments model 600A potentiostat (Austin TX) or a model 604B potentiostat. An electrochemical cell similar to that described by Chidsey is used for all electrochemical measurements on gold substrates[1]. It is a single-compartment, three-electrode glass cell consisting of a gold slide working electrode, a platinum counter electrode, and an Ag/AgCl reference electrode. A diagram of the setup is shown in figure 2.2. All potentials are quoted versus Ag/AgCl. The surface area of the working electrode is 0.65 cm^2 for these measurements, which is defined by the area of an O ring that contacts with the gold substrate. Surface roughness was determined using Porter's method and found to be 1.2[2]. Surface coverage reported here is accounted for considering this roughness. Solution resistance was compensated 80-100% using positive feedback IR compensation. All solutions were prepared in nano-pure water (18 MΩ · cm) and deareated with a nitrogen bubbler for 10

minutes prior to use. Different electrochemical measurements were conducted on different samples.

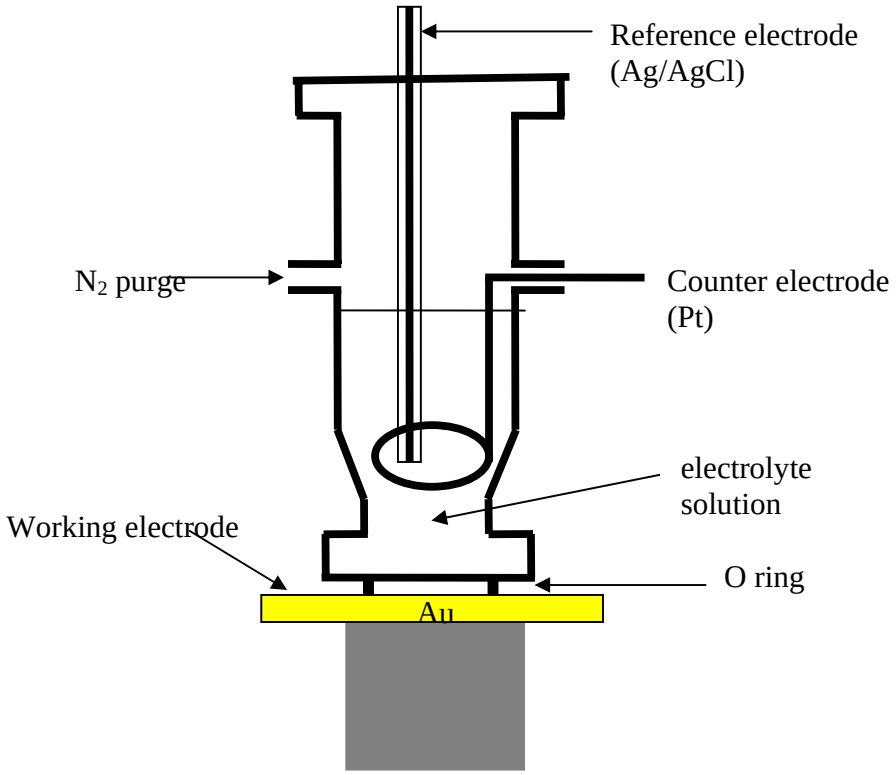

Figure 2.2. Electrochemical cell used for the electrochemical measurements on gold substrate. The electrolyte solution was contained within the cell by compression of O-ring.

2.2.1 Cyclic Voltammetry

Cyclic voltammetry was conducted using different conditions for samples prepared in different ways. Reductive desorption experiments were conducted on gold substrates covered by aminothiolphenol SAMs and (mercaptophenyl)phthalimide SAMs (both 3- and 4-) using a 0.5 M potassium hydroxide solution as the electrolyte. KOH was electronic grade (Aldrich) and used as received. In these experiments the potential was

swept from – 0.4 V to – 1.0 V at a rate of 50 mV/s. Reductive desorption measurements provide information regarding the surface coverage of thiols and the strength of the lateral interactions within a given monolayer[3]. Oxidation of the amine groups of aminothiophenol molecules were carried out on gold substrates covered by monolayers prepared by reaction of the aminothiophenol with the anhydride. The reaction on the surface was confirmed by the disappearance of the oxidation peak. 1 M sulfuric acid solution was used as the electrolyte. The potential was swept between 0 V and 1.0 V at a rate of 100 mV/s. All cyclic voltammetry data were acquired and processed with the software package supplied by EG&G.

2.2.2 Electrochemical Impedance Spectroscopy

Electrochemical impedance spectroscopy (EIS) measurements were performed on gold slides and copper electrodes to obtain the ionic insulating properties of the SAMs on gold slides and the protection ability of SAMs against corrosion of copper, respectively. Figure 2.3 is schematic of electrochemical setup for electrochemical impedance measurements. A three-electrode potentiostat (CH Instruments model 604B) is used for these measurements. All experiments were conducted at room temperature. Here, all impedance spectra were recorded at a fixed sample potential and then fitted to circuit models for impedance analysis. Complex nonlinear least squares (CNLS) fitting of data were performed using LEVM software version 8.0.

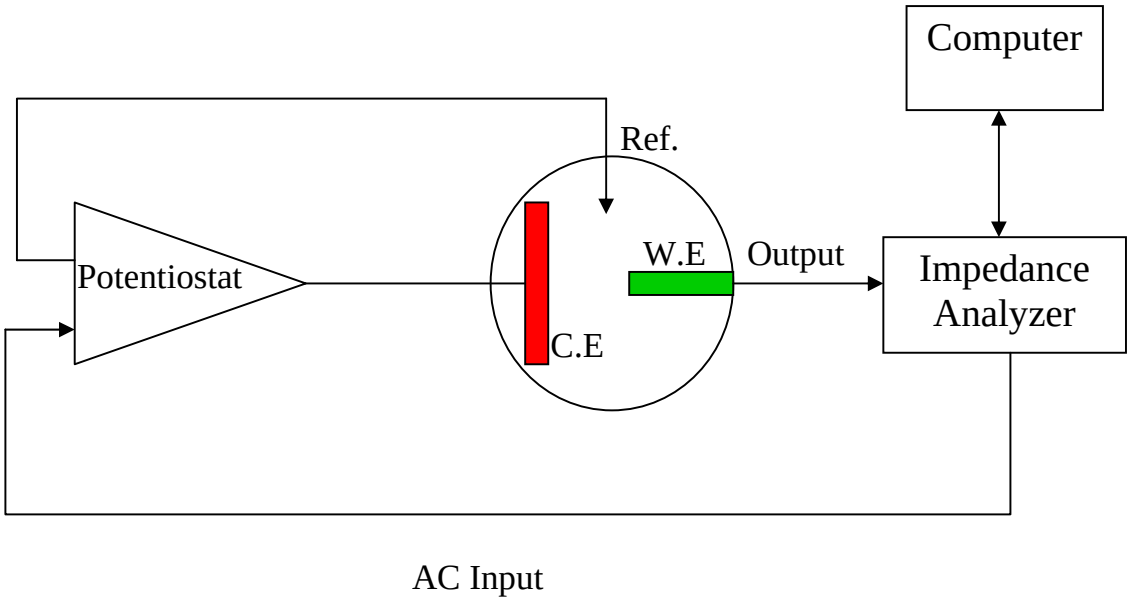

Figure 2.3. Schematic of electrochemical setup for impedance measurements.

2.2.3 Polarization Measurements

Polarization measurements of copper electrodes, both bare and covered with 3- and 4-MPP SAMs, were carried out potentiostatically in 0.2 M NaCl solution at room temperature. When the open-circuit potential of the bare electrode or SAMS-covered copper electrodes tended to a stable value, the potentiodynamic polarization curves were begun to record from the cathodic to the anodic potentials at the scanning rate of 0.2 mV/s from -0.4 to 0 V.

2.3 Contact Angle Measurements

Contact angle measurements are a simple and effective method to determine the surface energies and wetting behavior. It gives a first impression about the structure and composition of the monolayers[4,5,6].

The contact angle of modified gold surfaces was measured with a Rame-Hart NRL contact angle goniometer using the sessile, static drop method. A diagram of the components of a sessile drop goniometer is shown in figure 2.4. Nanopure water purified from a Barnstead Nanapure II water purification system with a measured resistivity of 18.0 MΩ cm was used as the probe liquid. Values reported here are the averages of at least 4 measurements per sample.

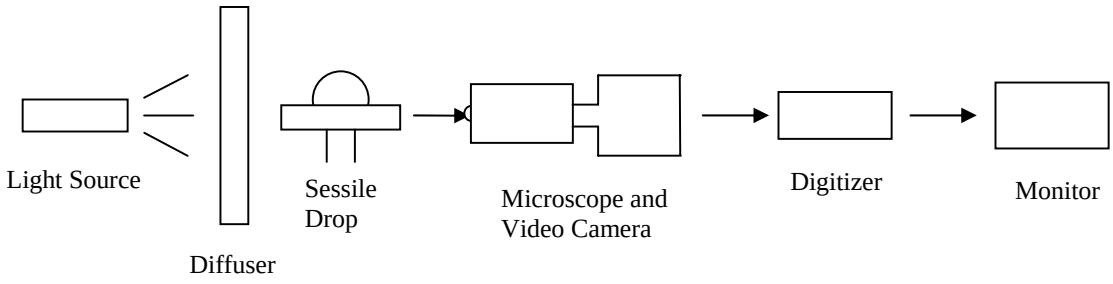

Figure 2.4. Diagram of components of a sessile drop goniometer.

2.4 Optical Ellipsometry

Optical ellipsometry was used to measure the change of the thickness of aminothiophenol SAMs on gold substrates before and after the reaction with phthalic anhydride. Ellipsometry data were collected with a Beaglehole picometer ellipsometer (Wellington, New Zealand). A photoelastic birefringence modulator was used with the modulation frequency set at 50 KHz. The light source was a HeNe laser (632.8 nm) and the detector was an end-on photomultiplier. Measurements were performed between 70° and 80° at 1° intervals. Substrate n and k values were obtained by analyzing bare gold data using spreadsheet. Beaglehole system software was used to simulate Δ and Ψ, and

ellipsometric thickness for each self-assembled monolayer was obtained by comparing the experimental data with the simulation value.

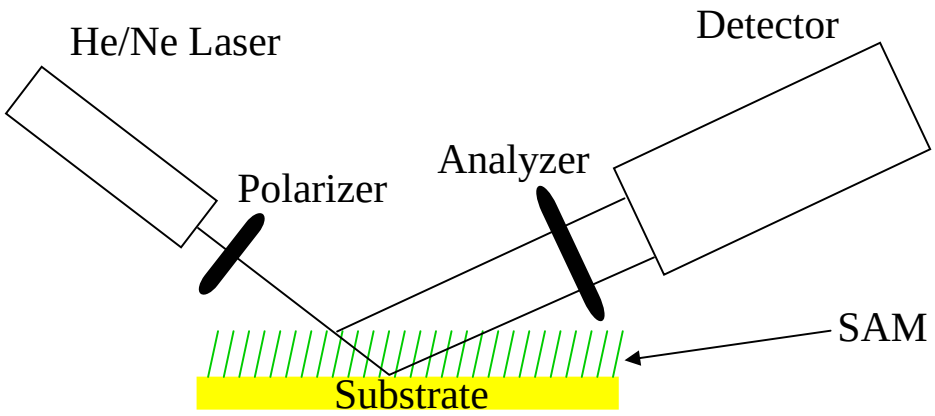

Figure 2.5. Schematic drawing of an ellipsometer

2.5 Materials

Gold slides were purchased from Evaporated Metal Films Inc. (Ithaca, NY). The substrates were 1 in. × 1 in. glass microscope slides with a 50 Å vapor deposited layer of Cr followed by a 1000 Å layer of Au vapor deposited on top of the Cr. 4-Aminothiolphenol (4-ATP), and 3-Aminothiolphenol (3-ATP) were purchased from Aldrich Chemical Co. and purified by column chromatography. (4-mercaptophenyl) phthalimide (4-MPP) and (3-mercaptophenyl) phthalimide (3-MPP) were synthesized in our lab using a literature procedure[7]. Phthalic anhydride (PA), acetic anhydride, triethylamine, supra pure sulfuric acid, potassium hydroxide (electronic grade),

concentrated sulfuric acid, 30% hydrogen peroxide, and sodium phosphate were obtained from Aldrich Chemical Co. and used as received.

2.6 SAMs Preparation

2.6.1. SAMs on Gold Slides

Gold slides were cleaned prior to use by soaking in piranha solution (3:1 conc. H_2SO_4:30% H_2O_2) for 10 minutes and then rinsed with water. Afterward, the clean gold slides were immersed immediately in a 2 mM chloroform solution of the mercapto. Self-assembling time of the thiols on the gold substrates depends on the experimental requirements. After being immersed in the thiols chloroform solutions for the designated time, the gold slides were taken out , rinsed with chloroform extensively and dried with a stream of nitrogen.

2.6.2. SAMs on Copper Electrodes

Preparation of Copper Electrodes. A 3.1 mm-diameter copper rod (Aldrich, 99.999%) was used for electrochemical experiments. The copper rods were embedded in epoxy resin mold (Epon 828), leaving only their cross-section exposed. The surface were prepared for self-assembly by immersing the copper electrode in the 3- and 4-MPP solutions.

Monolayer Self-Assembly. The copper surface was first ground with SiC abrasive papers of decreasing particle size to 1500 grit finish, rinsed with deionized water, polished with 1μ and 0.05μ alumina, rinsed with deionized water again, degreased with acetone, dried in a stream of nitrogen stream, and then etched in 7 M HNO_3 solution for

20 seconds to obtain the fresh, oxide-free cupper surface. The etched copper surface was rinsed with deionized water and acetone rapidly, and finally immersed in deoxygenated acetone solutions containing 2 mM of the thiols immediately. Before and during immersion, the thiols solution was purged with high pure N_2. Immersion time depended on the experimental requirement.

2.7 References

1 . Chidsey, C.E.D.; Loiacono, D.N. *Langmuir* **1990,** *6,* 682

2 . Porter, M.D.; Bright, T.B.; Allara, D.L.; Chidsey, C.E.D. *Journal of the American Chemical Society* **1987,** *109,* 3559

3. Imabayashi, S.; Iida, M.; Hobara, D.; Feng, Z.Q.; Niki, K.; Kakiuchi, T.J. *Journal of Electroanalytical Chemistry* **1997,** *428,* 33

4. Adamson, A.W. *physical Chemistry of Surfaces,* Wiley, Chichester, UK **1993**

5. Ulman, A. *An Introduction to Ultrathin Organic Films: From Langmuir-Blodgett to Self-Assembly,* Academic Press, Boston **1991**

6. Bain, C.D.; Whitesides, G.M. *Angew. Chem. Int. Ed. Engl* **1989,** *28,* 506

Chapter 3

Reactivity of Self-assembled Monolayers of 3-Aminothiophenol and 4-Aminothiophenol toward Phthalic Anhydride on Gold Substrates

3.1 Introduction

Polyimides are a class of high-temperature polymers extensively used in microelectronics and composites due to their excellent thermal and mechanical stability, low dielectric constants, and chemical resistance. While strong and durable bonds between polyimides and substrates are stringently required in these applications, it is generally found that polyimides have poor adhesion to metal substrates, especially when they were exposed to warm, humid environments. A few investigations to study the molecular structure of polyimide/substrate interphases have been reported in order to optimize the performance and stability of polyimide/substrate joints[1,2,3,4]. In these studies, polyimide/substrate interphases were formed by curing the polyamic acids.

Another common technique for improving adhesion in polyimide/metal systems is the application of a coupling agent to the adherend surface. Organosulfur compounds are promising candidates for use as coupling agents because of strong chemical interactions between the sulfur atom and metals such as gold, silver, and copper. One approach is to incorporate the sulfur-containing groups into the polymers or oligomers prior to the deposition of films onto the metal substrates[5,6]. Another approach for introducing sulfur-containing species into the polymer-metal interface is to pretreat the metal substrate with self-assembled monolayers, such as aminophenyldisulfide and aminothiophenol [4,7,8].

Functional groups at the outer layer of these monolayers can then further react with polymers, forming chemical bridges between the polymer and the metal, leading to improved adhesion. Young and co-workers studied phthalic anhydride (PA)/4-aminophenyl disulfide (APDS)/Au systems and PA/*meta*-aminothiophenol (m-ATP)/Ag systems using surface-enhanced Raman scattering (SERS) and RAIR to address the interaction between polyimide model compounds and organosulfur functionalized metal surfaces[7,8]. When PA was deposited onto a gold substrate covered by APDS SAMs or onto a silver substrate covered by m-ATP SAMs, the anhydride groups of PA reacted with the amino groups of APDS or m-ATP to form amic acids. Chemical curing of these amic acids in different solvent produced mainly either isoimide or imide species on the surface.

Here we report investigations of reactivity of self-assembled monolayers of 4-aminothiophenol (4-ATP) and 3-aminothiophenol (3-ATP) toward PA on gold substrates. Procedures similar to Young's[7,8] were used to form imide species on gold substrates pretreated with 4-ATP and 3-ATP SAMs. RAIRS, contact angle measurements, electrochemistry, and ellipsometry were applied to verify the reactions and to determine the yield of the reactions. A brief introduction to each technique is given here. Our RAIRS results showed that imide was the predominant product in both cases. Because different techniques have different sensitivity to the structural features and different averaging behaviors, different characterization methods give out different reactivities. No conclusive results were obtained here.

Reflection-Absorption Infra-Red Spectroscopy (RAIRS)

RAIRS has developed into one of the primary methods of monitoring chemical structure and molecular orientation of thin films and monolayers adsorbed onto metal surfaces. Francis and Ellison first applied RAIRS to characterize the system of Langmuir-Blodgett (LB) films of metal stearates on metal mirrors in 1959[9]. Because the spectrum is completely different from that obtained by reflection from the surface of a bulk sample, the term RAIRS was first suggested by Greenler *et al.* to refer specifically to the method of obtaining the spectrum of a thin layer of material located on the highly reflecting surface of a metal[10]. In order for light of wavenumber, κ, to be absorbed by a molecule, the molecule must have a nonzero dipole transition moment at that frequency ν, the magnitude of the electric vector of the light must be nonzero in the region of the molecule, and the molecule must also have a nonzero component of its dipole transition moment along the direction of the electric vector of the light.

The work of Greenler and others showed that the RAIR spectrum of thin films and monolayers covering metal substrates depended on the optical constants of the adsorbate and substrate, the angle of incidence, and state of polarization of the incident infrared beam[9,11,12,13,14]. When the light is reflected from a metal surface, the electric vector of the incident light suffers a phase change on reflection which depends on the angle of incidence and the state of polarization of the incidence light. The phase shift for the s-polarized beam (with the electric vector perpendicular to the plane of incidence) is not a strong function of the angle of incidence, remaining near 180° for all angles of incidence as shown in figure 3.1. Therefore, the electric vectors of the incident and reflected beams nearly cancel out at the surface, resulting in very little absorption from a

thin layer on a metal for an s-polarized beam would be expected, irrespective of the orientation of the transition dipole. However, the phase shift for the p-polarized beam (with the electric vector parallel to the plane of incidence) is a strong function of the angle of incidence, varying from near 0° at small angles of incidence to 180° at grazing incidence. At a near grazing incidence angle where the phase shift is 90°, the vector addition of the incident and reflected electric vectors results in a stronger electric field perpendicular to the metal surface as shown in figure 3.1. Therefore, the p-polarized beam is strongly absorbed by a transition dipole moment oriented perpendicular to the film surface. This gives rise to a "surface selection rule": only vibrations having a component of their transition dipole moment perpendicular to the substrate surface are observed in the reflection infrared spectrum. So in the experiments, a p-polarized infrared light is introduced onto the surface at near grazing incidence angle and reflected from the surface to the detector. Combining the surface selection rule with experimental signal intensities, the orientation of the organic molecules composing the self-assembled monolayer can be determined with respect to the substrate surface.

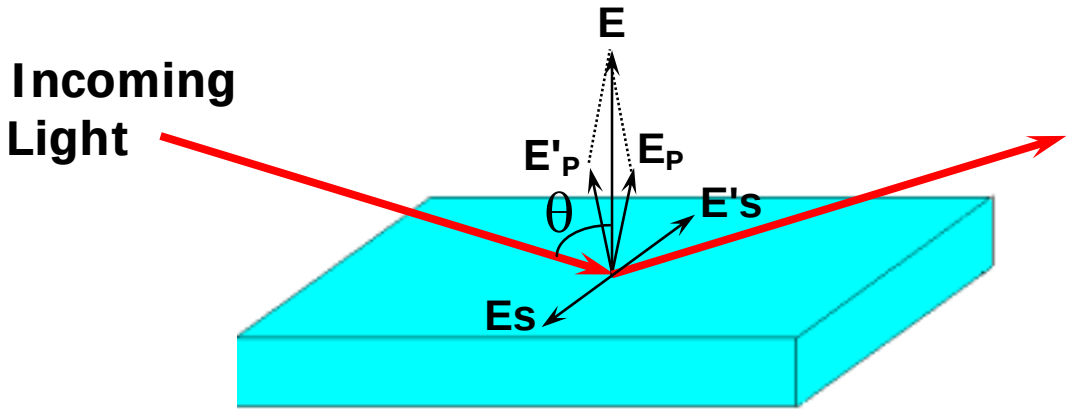

Figure 3.1 Sum of the incident and reflected electric vectors for s- and p-polarizations.

The dependence of the reflection equations for a air-monolayer-metal three phase system on the angle of incidence and polarization of the incident radiation were calculated by considering the boundary conditions of an electromagnetic wave in each medium[11,13,15,16,17,18]. An absorption factor A_ν was defined as:

$$A_\nu = 1 - \frac{R_\nu^d}{R_\nu^0} \qquad (3.1)$$

where ν = s or p. R_ν^0 is the reflectance of the bare substrate and R_ν^d is the reflectance of the three phase system. The calculated results showed that the optimum angle of incidence for an RAIRS experiment is near grazing incidence, and only the p-polarized beam is absorbed at the optimum angle ($A_p \approx 10^5 A_s$). An angle of incidence of 80° was used in our experiments.

Contact Angle Measurement

Contact angle measurement is a simple-to-adopt physical surface analytical method widely used for determining the surface energy properties of solid materials[19]. Several methods were used to measure contact angle but only the sessile drop method was used here. Contact angle describes the shape of a liquid droplet resting on a solid surface. When drawing a tangent line from the droplet to the touch of the solid surface, the contact angle is the angle between the tangent line and the solid surface, as illustrated in figure 3.2. The drop of liquid forming an angle may be considered as resting in equilibrium by balancing the three forces involved. Namely, the interfacial tensions between solid and liquid (γ_{SL}), that between solid and vapor (γ_{SV}), and that between liquid and vapor (γ_{LV}). When a droplet of a high surface tension liquid rests on a solid of low surface energy, the liquid surface tension will cause the droplet to form a spherical shape (lowest energy shape). Conversely, when the solid surface energy exceeds the liquid surface tension, the droplet is a flatter, lower profile shape.

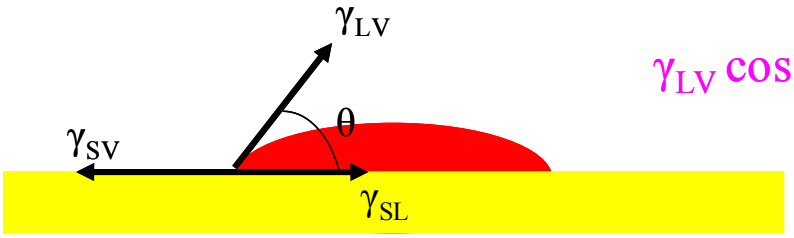

Figure 3.2 Surface tension components of a liquid drop on a surface of a solid material in equilibrium

Traditionally, contact angle measurements utilize a sample stage to hold the substrate, a syringe to apply a droplet of liquid, a light source to illuminate the droplet, and a set of optics for magnifying the image for observation. Typically a goniometer as depicted in figure 2.4 is used. If a liquid with well-known properties is used, the resulting interfacial tension can be used to identify the nature of the solid. This technique is extremely surface sensitive, with the ability to detect properties on monolayers. The contact angle can be used to detect the presence of films, coating, or contaminants with a surface energy different from that of the underlying substrate.

Electrochemistry

Electrochemistry measurements are useful techniques for the analysis of surface bound compounds. The electrochemical characterization of SAMs on gold substrates is often performed by cyclic voltammetry (CV)[20]. Large potential sweeps on the order of 0.1 V to 1 V are applied to the SAMs modified gold electrode and the resulting current is recorded. CV can be used to determine several properties of SAM surfaces such as the surface coverage of SAMs[21,22], the strength of the lateral interactions with SAMs[21], the average thickness of the SAMs, the size and number of defects in SAMs[23,24]. SAMs which have an electro-active tail groups can also be identified by CV[25,26]. Here, we conducted CV experiments on 3- and 4-ATP SAMs modified gold substrates before and after reaction with phthalic anhydride. Change of the intensity of the oxidation peak of amino groups in the SAMs provided an evidence of the reaction on the surface.

Ellipsometry

Ellipsometry is a non-destructive optical technique, which deals with the measurement and interpretation of the state of polarized light undergoing reflection from a sample surface. Because the optical properties and composition of the substrate and overlayer (their thickness and morphology, and surface roughness) determine the reflection coefficients, ellipsometry is exploited as a non-invasive probe of the refractive index and thickness of thin films.

The quantities measured by an ellipsometer are ellipsometric angles ψ and Δ which are related to the complex reflectance ratio ρ of the Fresnel reflection coefficient Rp and Rs for light polarized parallel (p) and perpendicular (s) to the plane of incidence such that

$$\rho = R_p / R_s = \tan\varphi \bullet \exp(i\Lambda) \qquad (3.2)$$

The complex reflectance ratio ρ is completely determined by amplitude ($\tan\psi$) and a phase Δ and characterize the differential changes in amplitude and phase. Phase information contained in Δ makes the ellipsometry measurement very sensitive.

Figure 3.3 shows a linearly polarized input beam is converted to an elliptically polarized reflected beam. For any angle of incidence between 0° and 90°, p-polarized light and s-polarized light will be reflected differently.

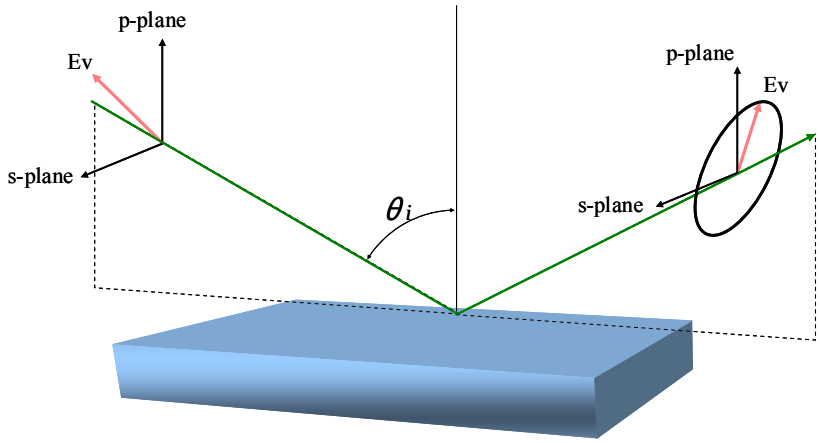

Figure 3.3 Schematic of the geometry of an ellipsometry experiment.

As ψ and Δ are dependent on the angle of incidence θ, wavelength λ, optical properties of all phases, and thickness of thin films, at least two measurements are required to get the refractive index and the thickness of thin films for a common single thin layer system when the refractive index of the surrounding medium and the angle of incidence θ are known, provided that the refractive index n is real. To find out the refractive index and the thickness of thin films, a fitting procedure is used for null ellipsometry with a fixed angle of incidence. Commonly, ellipsometry measurements were done at multiple angles of incidence.

3.2 Experimental Details

3.2.1 thiol-terminated imide synthesis[27]

Phthalic anhydride, 4-ATP, and 3-ATP were dissolved in *N*,*N*-dimethylacetamide (DMAc) in glass sample bottle capped and purged with nitrogen. A two-necked round bottom flask equipped with nitrogen inlet and a condenser was used as the reaction vessel.

The proton NMR spectra were obtained by a Varian Inova 400 MHz spectrometer. High resolution mass spectra were obtained by a JEOL HX100 spectrometer.

(4-mercaptophenyl)phthalimide (4-MPP). Equal molar amounts of phthalic anhydride and 4-aminothiophenol solutions were injected into the reaction vessel and mixed together. The mixture was refluxed at about 160 ºC overnight and then cooled to room temperature. The pale yellow precipitate which formed was filtered, rinsed with copious amounts of ether, vacuum dried for several hours to remove residual solvents, and purified by recrystalization in chloroform.

(3-mercaptophenyl)phthalimide (3-MPP). Equal molar amounts of phthalic anhydride and 3-aminothiophenol were injected into the reaction vessel and mixed together. The mixture was refluxed overnight at about 135 °C and then cooled to room temperature. The reaction solution turned to orange but unlike the synthesis of (4-mercaptophenyl)-phthalimide, no precipitate was formed from the reaction mixture. Water and chloroform were then added to the reaction mixture to extract the product and unreacted reactants into chloroform and to remove DMAc to the water layer. Chloroform was removed and yellow (3-mercaptophenyl)-phthalimide was purified by column chromatography using an elution solvent of 5:1 hexane/ethyl acetate.

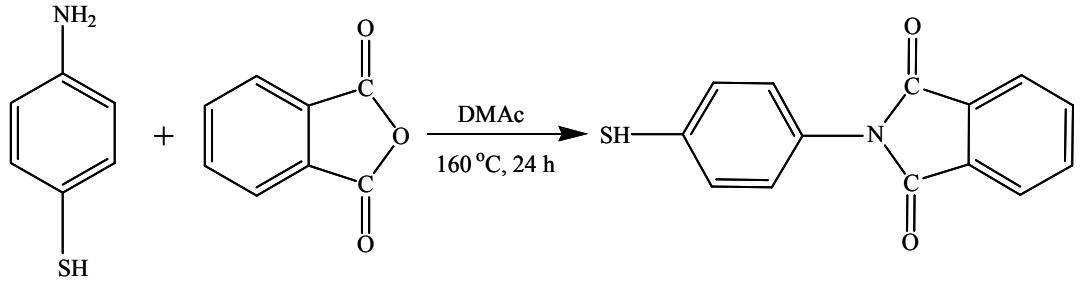

4-ATP PA 4-MPP

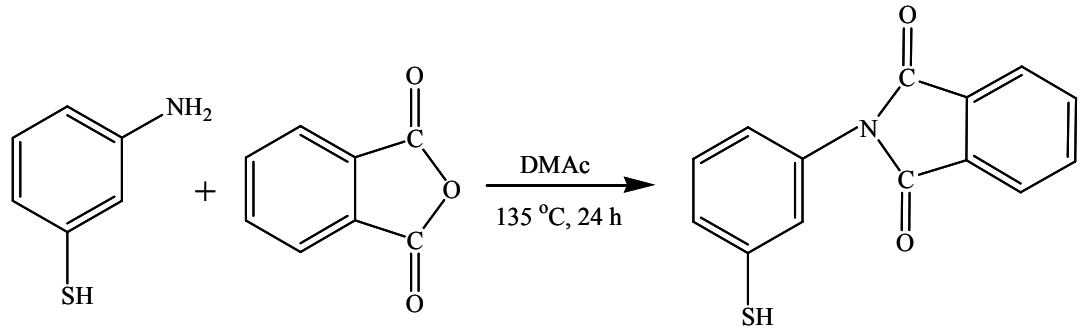

3-ATP PA 3-MPP

Scheme 3.1. Synthesis of thiol-terminated imides

3.2.2 Reaction on gold substrates

A similar procedure as Young's was used here with some modifications on solution concentration and substrate soaking time[6,7]. Formation of imides on the 3-ATP or 4-ATP-coated gold substrates was made by a two-step reaction at room temperature as shown in scheme 2. First gold substrates modified with 3-ATP or 4-ATP SAMs by immersion in 2 mM thiol chloroform solution overnight were immersed in a 0.2%

solution of PA in chloroform for two days and rinsed with chloroform. Anhydride groups of PA reacted with amine groups of 3- or 4-ATP to form amic acids on the gold surface. After that, substrates were immersed in mixtures of acetic anhydride and triethylamine (1:1 ratio by volume, prepared under the nitrogen environment at room temperature) for at least four days. Amic acid films were chemically cured to imides (3-MPP and 4-MPP, respectively) in acetic anhydride using triethylamine as a catalyst.

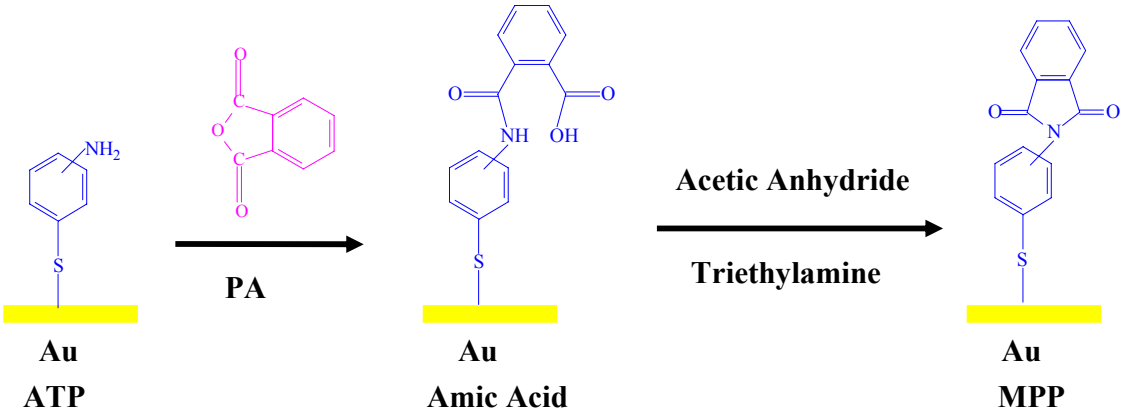

Scheme 3.2. Representation of proposed reaction procedure.

3.2.3 Single component and mixed SAMs preparation

To investigate the efficiency of the reaction of the ATP monolayers, mixed self-assembled monolayers of 4-ATP and 4-MPP, 3-ATP and 3-MPP were prepared by the simultaneous adsorption from mercaptan solutions where the total mercaptan concentration was 0.002 M. Clean gold substrates were immersed in the thiol solution overnight to prepare the monolayer.

3.3 Results and Discussion

3.3.1 Reflection-Absorption Infra-Red Spectroscopy (RAIRS)

Figure 3.4 are RAIR spectra of 4-ATP monolayers before and after reaction toward phthalic anhydride in the range of 1300 cm^{-1} to 1850 cm^{-1}. The upper trace shows the RAIR spectrum of a 4-ATP monolayer prepared by immersing the gold substrate in 4-ATP chloroform solution overnight. Three prominent absorptions are observed here. The band near 1626 cm^{-1} was assigned to the bending mode of NH_2 groups (δ_{NH} mode)[28]. Other two bands were related to vibrational modes of para-substituted benzene rings. Bands near 1586 cm^{-1} and 1490 cm^{-1} were assigned to C-C stretching 8a and 19a modes (ν_{CC} modes), respectively, using the Wilson numbering system[29,30]. The observed frequencies are essentially identical to what have been observed for 4-ATP on Au and Ag surfaces[7,31,32]. The lower trace in the spectra was obtained from a 4-ATP monolayer after reacted toward phthalic anhydride. The most striking differences between the two spectra are the appearance of an intense band at 1380 cm^{-1} and the disappearance of NH_2 group bending mode at 1626 cm^{-1} in the spectrum of monolayer reacted with phthalic anhydride. The 1380 cm^{-1} band was assigned to CNC axial stretching in the imide II band. A strong band near 1380 cm^{-1} and a very weak band near 1780 cm^{-1} that associated with vibrational modes of imide groups were observed in the spectrum, while bands near 1224, and 1690 cm^{-1} related to isoimide groups were not observed in the spectrum. This result implied that imide was the predominant product when curing with triethylamine catalyst, in agreement with Young's work[7]. In addition, two C-C stretching bands were also observed, changing in intensity.

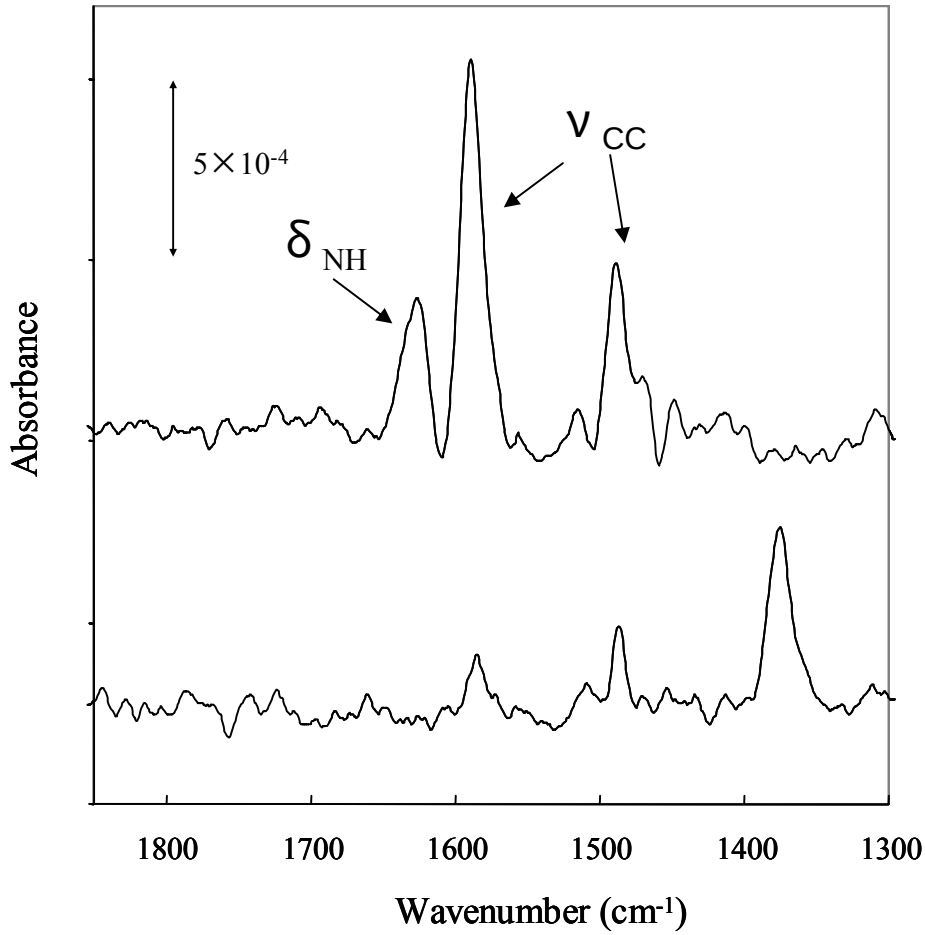

Figure 3.4. RAIR spectra of 4-ATP monolayers modified gold substrates before and after reaction toward phthalic anhydride. The upper trace is the RAIR spectrum of a 4-ATP monolayer. The lower trace is the RAIR spectrum of a 4-ATP monolayer after reacted with phthalic anhydride.

Figure 3.5 are RAIR spectra of 3-ATP monolayers before and after reaction toward phthalic anhydride in the range of 1300 cm^{-1} to 1850 cm^{-1}. The upper trace is spectrum of 3-ATP monolayers and the lower trace is spectrum of 3-ATP monolayers after reacted toward phthalic anhydride on gold substrate.

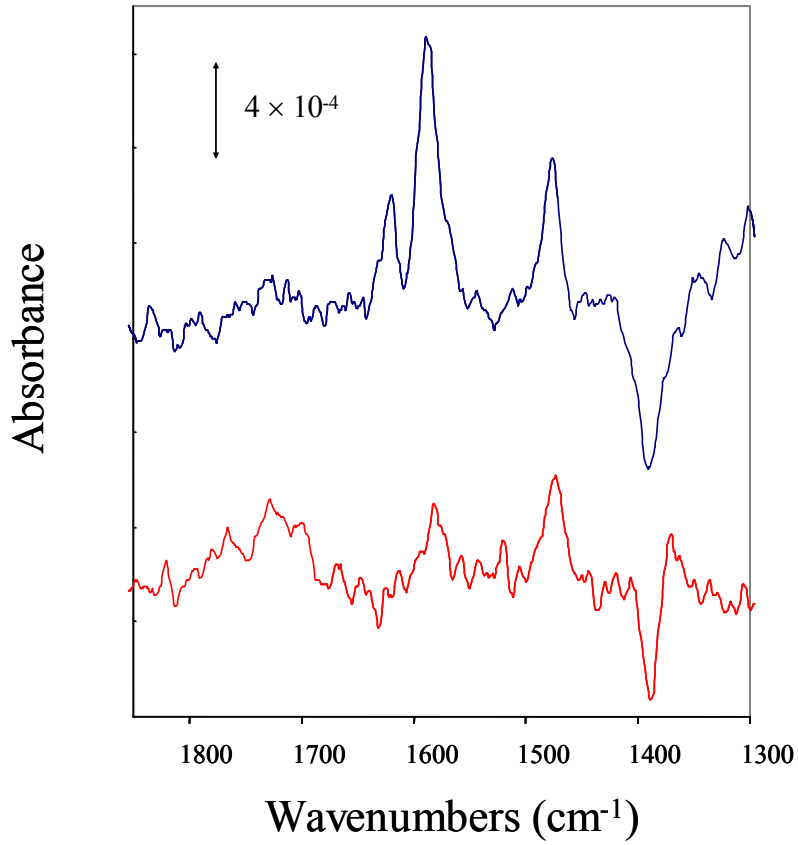

Figure 3.5. RAIR spectra of 3-ATP monolayers on gold substrates before and after reaction toward phthalic anhydride.

RAIRS of 3-ATP monolayers also showed same three prominent absorptions at 1626, 1586, and 1490 cm^{-1} as 4-ATP monolayers and assigned to the δ_{NH} (1626 cm^{-1}) mode and the ν_{CC} (1586 and 1490 cm^{-1}) modes, respectively, using Wilson numbering system. The observed frequency and relative band intensities are essentially identical to what has been observed for 3-ATP monolayer adsorbed onto a thick silver film[8]. The appearance of 1380 cm^{-1} band related to imide groups and the disappearance of 1626 cm^{-1}

band related to NH_2 groups were again observed in the spectrum obtained from 3-ATP monolayer after reacted toward phthalic anhydride. IR bands associated with isoimide near 1685 cm^{-1} was not observed in this spectrum. Our results indicated that imide was the predominant product when the sample was cured with triethylamine and acetic anhydride. This result is different from Young's work[8]. Their SERS spectra and RAIR spectra implied that isoimide was always the predominant product on both Au and Ag substrates no matter samples were cured with triethylamine catalyst or pyridine catalyst, demonstrating that the metal substrate did not play an important role in the chemical curing of the model system. Compared with their results of curing PA/APDS/Au systems in acetic anhydride/triethylamine solutions, they concluded that the effect of substituents attached to the benzene rings of organosulfur compounds on the composition of curing products was critical in the model systems. They discussed the results based on the same mechanism as formation of imide in the bulk. Imide groups were mostly produced by the rearrangement of isoimide to imide involving a transition state in which the negative charges were developed on the N atom[33,34,35,36]. All monolayer molecules were chemisorbed on the metal surface through S atoms. The electron withdrawal from a para-substituent (the nitrogen atoms in these cases) resulted from the interaction of S lone-pair electrons with metal stabilized by the transition state and this favored the isoimide-imide rearrangement; therefore, the imide became the predominant product. The isoimide-imide rearrangement, however, was not favored for a meta-substituent because the chemisorbed S-metal bond would not cause electron withdrawal and isoimide became the predominant product.

The reason our predominant product was imide while Young's was isoimide might be the different curing time. We cured the amic acid specimens in a mixture of acetic anhydride and triethylamine for several days which was much longer than Young's 24 hours. A mixture of isoimide and imide was observed in their spectra, but the intensities of isoimide bands were much stronger than that of imide band. Their results suggested that the reaction rate of isoimide-imide rearrangement was very slow. By extending the curing time, we got imide as our predominant product.

To probe the reactivity of 3-ATP and 4-ATP monolayers toward phthalic anhydride on gold substrates, we examined the behavior of two-component monolayers formed from co-adsorbed 3-ATP and 3-MPP, or 4-ATP and 4-MPP, respectively. Two component surfaces were studied using RAIRS and contact angle measurements.

Figure 3.6 is the RAIR spectra of 4-ATP/4-MPP mixed monolayers in the 1300 – 1850 cm^{-1} region. The characteristic bands were assigned as we discussed above. The mole fraction of 4-MPP in the chloroform thiol solution, $X_{4\text{-MPP}}(soln)$, is given for each spectrum. The mole fraction of 4-MPP in the mixed monolayers was not determined. The intensities of imide bands increased as mole fraction of 4-MPP in solution also increased, while the intensities of amine bands showed a trend toward decreasing. The intensity of imide band obtained from monolayers prepared in the solution containing 0.25 mole fraction of 4-MPP was almost half of that obtained from 4-MPP solution, and did not increase much when the mole fraction of 4-MPP increased from 0.25 to 0.75. These results indicated that the transfer ratios of the two adsorbates are not equal. 4-MPP is preferentially adsorbed on the gold substrate. To use RAIR spectra of mixed monolayers to determine the reactivity of 4-ATP monolayer toward phthalic anhydride, the mole

fraction of 4-MPP in the mixed monolayer must be determined provided that the orientation of molecules on the deposited monolayers and the reacted monolayers was the same.

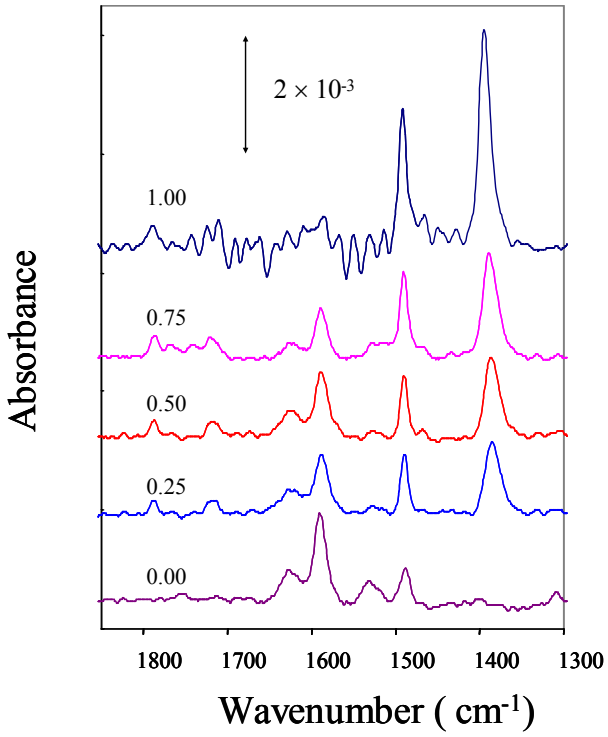

Figure 3.6. RAIR spectra of 4-ATP/4-MPP mixed monolayers as a function of the 4-MPP concentration in the chloroform solution, $X_{4\text{-MPP}}$(soln). The value of $X_{4\text{-MPP}}$(soln) is given for each spectrum.

RAIR spectra of 3-ATP/3-MPP mixed monolayers deposited from chloroform solution containg different mole fractions of 3-MPP were shown in figure 3.7. An intense band near 1730 cm^{-1} was observed in the 3-MPP spectrum. This band was assigned to the asymmetric vibration of the C=O groups in the imide I band and was not observed in the

4-MPP spectrum. This is due to the orientation of rigid aromatic thiol molecules and the surface selection rule of IR spectroscopy. As discussed previously, only the transition dipole moment perpendicular to the surface can be coupled with p-polarized light. Aromatic thiols were reported to have an adsorption geometry with a phenyl ring oriented almost normal to the Au surface and resulted in a more perpendicular transition dipole moment of imide I mode in 3-MPP molecules than that of 4-MPP molecules because of their different substitution pattern. The intensities of the imide I band also showed a preferential adsorption of 3-MPP molecules to 3-ATP molecules. Unlike 4-MPP/4-ATP mixed monolayers, the imide II band near 1380 cm^{-1} was almost disappeared in the spectra 3-MPP/3-ATP mixed monolayers. The reason is not clear.

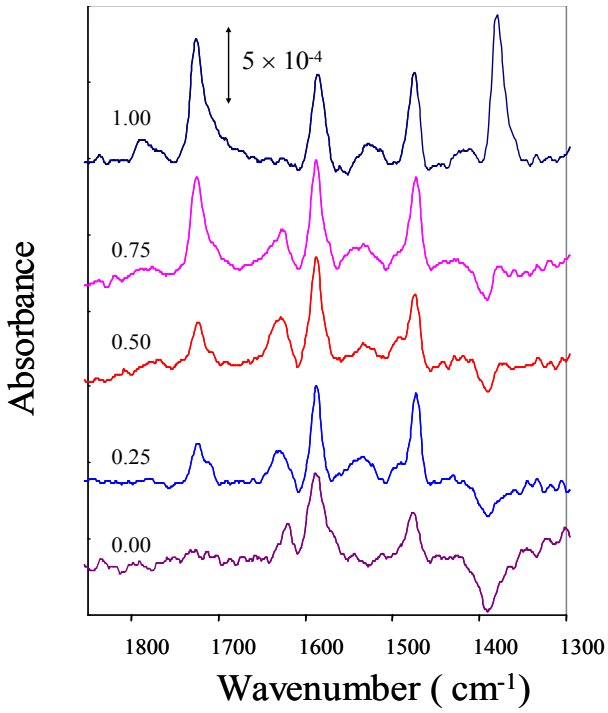

Figure 3.7. RAIR spectra of 3-ATP/3-MPP mixed monolayers as a function of the 3-MPP concentration in the chloroform solution, $X_{3\text{-MPP}}$(soln). The value of $X_{3\text{-MPP}}$(soln) is given for each spectrum.

3.3.2 Electrochemistry Measurements

Hayes and Shannon studied the cyclic voltammetry of 4-ATP monolayer adsorbed on an Au electrode in 1 M $HClO_4$ solution and proposed ECE mechanism for the electrooxidation of 4-ATP monolayers[37]. They assigned the initial irreversible oxidative wave in the first cycle to the oxidation of adsorbed 4-ATP in its protonated form to the radical cation as shown in scheme 3. Mandler and co-workers investigated electrochemical behavior of the isomers of ATP[26]. Although different electroactive products were suggested, they were in agreement with the oxidation of the amino group in the first cycle. Some amino groups on the ATP monolayers should be converted to imide groups after ATP monolayers reacted with phthalic anhydride. Because the imide group is not electroactive in strong acidic solution between 0 – 1.0 V, the intensity of oxidation wave on the ATP modified surface is expected to decrease on the reacted surface if the reaction does happen, and probably provide us some quantitative information about the reactivity based on the intensity of the oxidation wave.

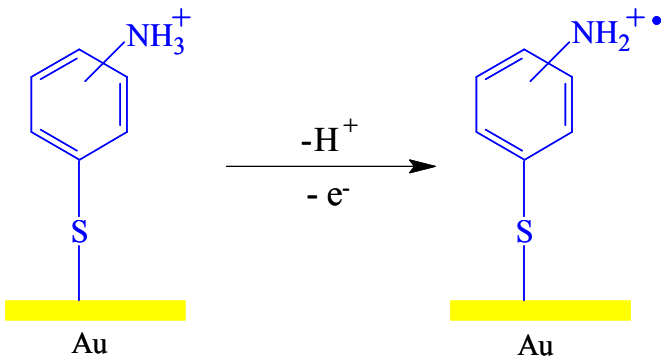

Scheme 3.3. Initial oxidation of amino groups in ATP monolayers on gold substrates.

The first cyclic voltammetry scan of 4-ATP and 3-ATP modified gold substrates before and after reaction with phthalic anhydride were shown in figure 3.8 and 3.9, respectively. The top trace is data collected with an unmodified gold surface. The voltammetry of bare gold surface was featureless when the potential was more negative than 1.0 V in 1.0 M H_2SO_4 electrolyte solution. The middle traces were voltammetry of 4-ATP and 3-ATP modified gold surfaces, respectively. 4-ATP monolayer showed a clear oxidation wave, while 3-ATP monolayer showed a small shoulder. Assuming a one electron oxidation, the surface coverage calculated by integrating the area under the oxidation wave of 4-, and 3-ATP correspond to 5.1 and 1.6×10^{-10} mol cm^{-2}. The charge due to 4-, and 3-ATP oxidation is significantly smaller than that reported by Mandler[26]. This result might be due to the differences in the modification procedure. While Mandler modified his gold substrates in an aqueous solution of 0.1 M sulfuric acid for 1 h under either continuous shaking or stirring, we formed our SAMs by soaking the gold substrate in chloroform solution for 24 h without any shaking or stirring. Moreover, STM images and XPS results alluded to the partial formation of more than a monolayer in Mandler's case.

While the coverage values for 4-ATP were higher than the surface coverage estimated from the reductive desorption (3.56×10^{-10} mol cm^{-2}) (that will be discussed in another chapter), the charge corresponding to the oxidation of 3-ATP was much smaller (3.6×10^{-10} mol cm^{-2}). It should be noticed that while in the reductive desorption experiments only molecules chemisorbed onto the surface through S-Au bond were desorbed, amino groups in molecules both chemisorbed and physisorbed onto the surface could be oxidized. Although the absolute values of the surface coverage from the

oxidation of amino groups were different, our results had the same order of the packing density as Mandler's results.

The bottom traces were the voltammetry on modified surfaces after reaction with phthalic anhydride and curing in acetic anhydride/triethylamine. No oxidation peaks were observed. This result suggests that amino groups in the ATP monolayers did react with phthalic anhydride; however, the percentage of the reaction could not be conclusively determined. Some factors might be taken into account here. The yield of the reaction might be high and leave only trace amount of un-reacted ATP molecules on the surface which could not be detected due to the detection limit of the instrument. On the other hand, the intermediate amic acid molecules and the product MPP molecules have bigger bulk than ATP molecules. This also make the amino groups of un-reacted ATP molecules hard to be detected. As no oxidation peak was observed on the reacted surface, the cyclic voltammetry were not done on the gold substrates modified with mixed monolayers.

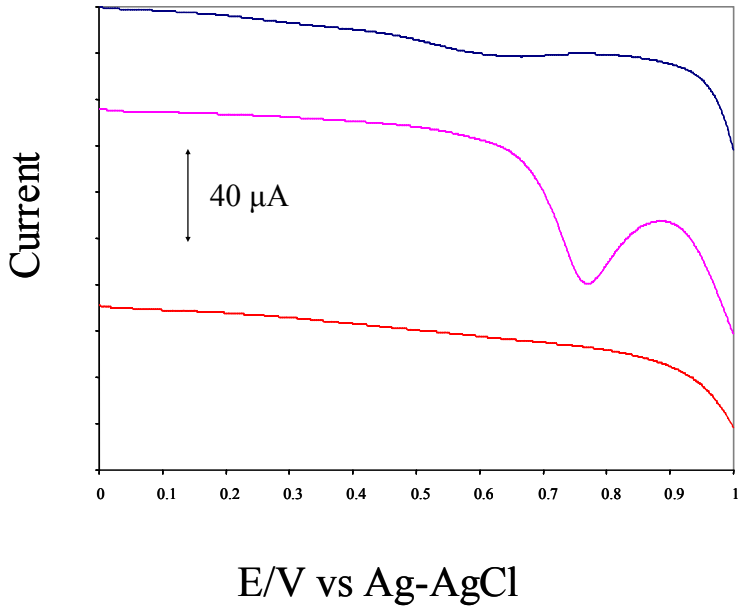

Figure 3.8. Electrochemical oxidation of amino groups on 4-ATP pretreated gold substrate before and after reaction with phthalic anhydride.

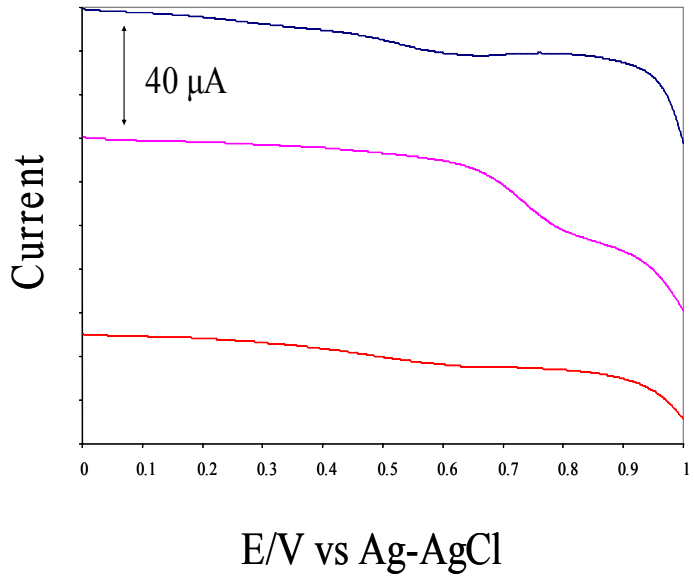

Figure 3.9. Electrochemical oxidation of amino groups on 3-ATP pretreated gold substrate before and after reaction with phthalic anhydride.

3.3.3 Contact Angle Measurements

Contact angle measurements are a simple and effective method to determine the surface energies and wetting behavior. It gives us a first impression about the surface composition of the monolayer. Considering the small tilt angle of the aromatic thiol monolayers on gold surface (about 15° to the surface normal), the different polarity of functional tail groups of ATP (polar amino group) and MPP molecules (non-polar benzene ring in imide), different orientation of tail groups in isomers due to the 60 degrees difference in the substitution at the 3 and 4 positions, 4-ATP monolayer should be the most polar one among the four SAMs, while 4-MPP the least polar one. The difference in polarity between 4-substituted molecules, 4-ATP and 4-MPP, should be much bigger than that of 3-substituted molecules, 3-ATP and 3-MPP. In the mixed monolayers, when the ATP molecules were replaced by the MPP molecules, the surface became less polar and had a lower surface energy.

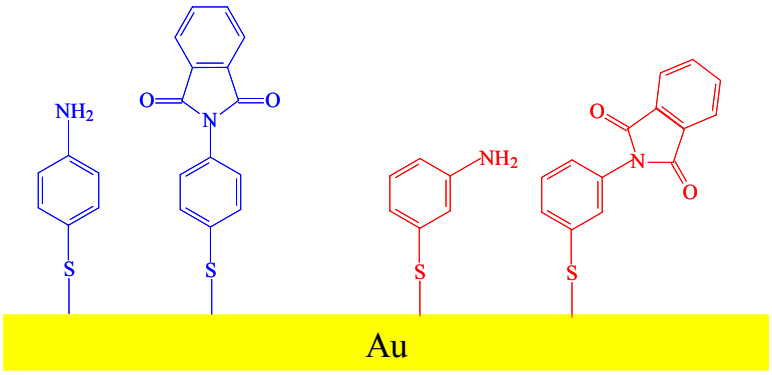

Scheme 3.4. Schematic drawing of four SAMs on gold substrate.

Contact angle measurement results of single-component SAMs, two-component SAMs and reacted surfaces are shown in figure 3.10. The results of single- and two-component monolayers were in good agreement with small tilt angles on the surface. The Contact angle of 4-ATP modified gold substrate increased from 43° to 70° after reaction toward phthalic anhydride, and increased from 47° to 61° for 3-ATP modified gold substrate. This big surface energy change indicated the reactions on the monolayer. The yield was estimated by comparing the contact angles of reacted surface with the mixed monolayers. The yield of 4-ATP monolayer was between mixed monolayers prepared from solution with mole fraction of 4-MPP 0.50 and 0.75, while the yield of 3-ATP monolayer was between 0.75 and 1.00. The contact angle data showed that reactivity of 3-ATP toward PA is a little bit higher than that of 4-ATP, provided that the surface composition of 4-ATP/4-MPP and 3-ATP/3-MPP mixed monolayers were the same if they were deposited from solution having the same mole fraction of MPP.

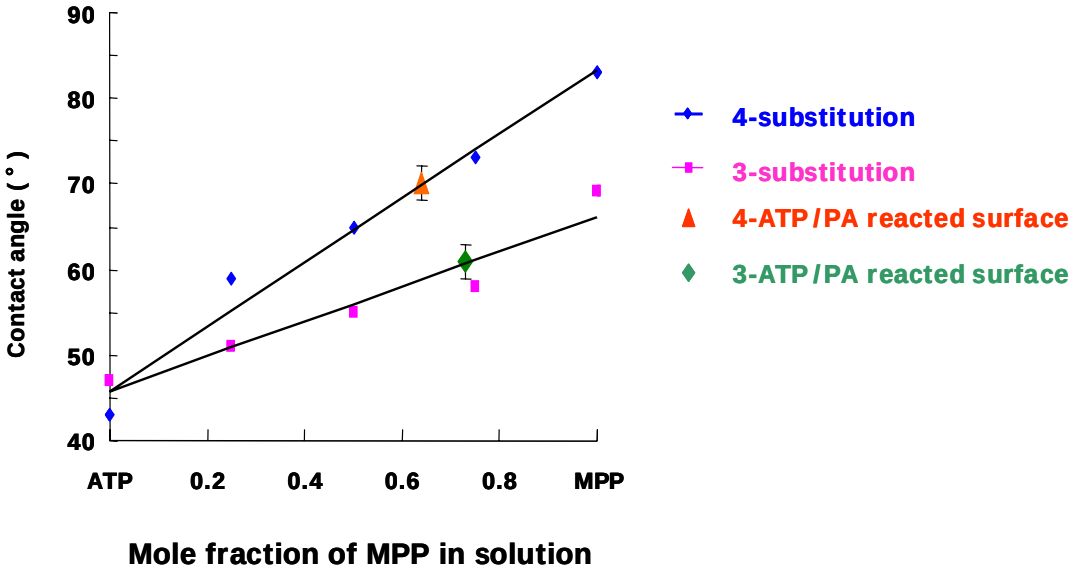

Figure 3.10. Contact angle of single component and two-component monolayers for 3- and 4-substitution molecules and ATP monolayers reacted with phthalic anhydride.

3.3.4 Ellipsometry Measurements

The optical constants of our gold substrate measured at a wavelength of 632.8 nm were n = 0.87 and k = 3.51. The thickness of four single component monolayers and reacted monolayers are summarized in figure 3.11. The thickness was retrieved from the simulation plot when those values for the optical constants of the gold substrate were used, a value of 1.4 for the refractive index of the monolayers was assumed, and the usual assumptions regarding uniform films with parallel sides were made.

MPP monolayers are expected to be thicker than the corresponding ATP monolayers because of the additional phenyl group. Considering the small tilt angle of monolayers and the different substitution patterns in 3- and 4-positions, the thickness different between 4-ATP and 4-MPP should be much bigger than that of 3-ATP and 3-MPP. These were confirmed by the ellipsometry results. When reacted with phthalic anhydride, the amino groups on ATP monolayers were replaced by bigger imide groups, therefore, the monolayer thickness should increase after reaction. Our results showed a big increase in 4-ATP monolayer, while the 3-ATP monolayer was almost the same before and after reaction. This is probably because we assumed the same refractive index for all monolayers. Actually, molecular structure, packing density and orientation of monolayer, etc. may affect the refractive index of monolayers. It is even more complicated on the reacted surface because of intermediates.

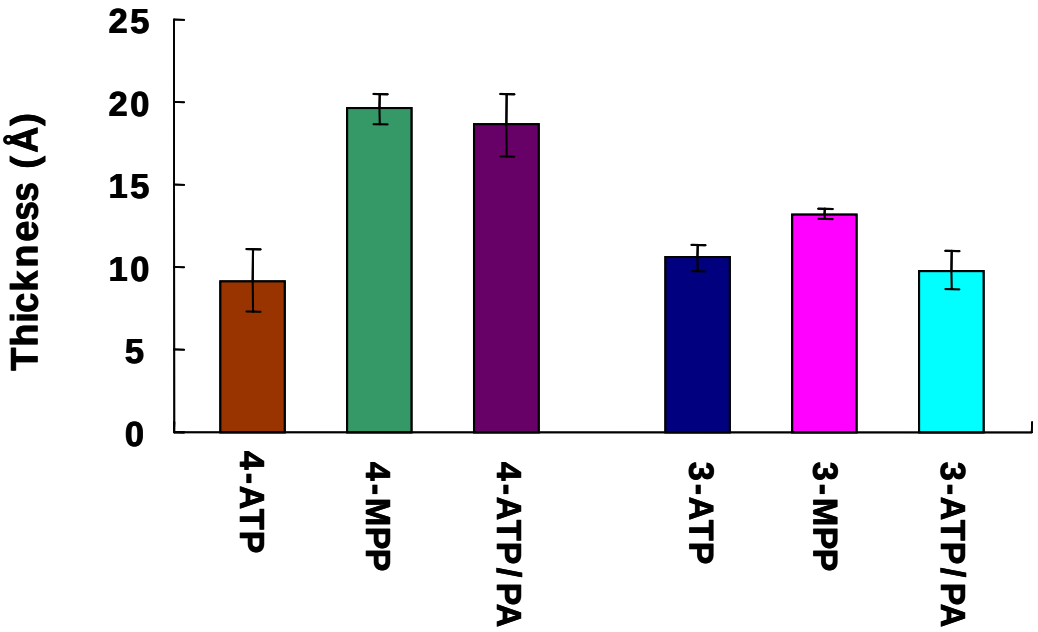

Figure 3.11. Ellipsometry Thickness of Single-component and Reacted Monolayers.

3.4 Conclusions

Reaction of ATP monolayers toward phthalic anhydride was investigated. Reflection absorption infrared spectroscopy, electrochemical oxidation of amine groups, and ellipsometry measurements demonstrate the covalent attachment of the anhydride. The efficiency of the reaction of the aminothiolphenol monolayers was investigated. Mixed self-assembled monolayers of 4-aminothiolphenol and (4-mercaptophenyl) phthalimide (4-MPP), 3-aminothiophenol and 3-MPP, were prepared by the simultaneous adsorption from solutions where the total mercaptan concentration was 0.002 M. The contact angle of the mixed monolayer increased with the increasing mole fraction of MPP

in the solution. The contact angle data shows that reactivity of 3-ATP toward PA is a little bit higher than that of 4-ATP.

3.5 References

1. Young, J.T.; Tsai, W.H.; Boerio, F.J. *Macromolecules* **1992,** *25,* 887

2. Tsai, W.H.; Boerio, F.J.; Jackson, K.M. *Langmuir* **1992,** *8,* 1443

3. Young, J.T.; Boerio, F.J. *Surface and Interface Analysis* **1993,** *20,* 341

4. Young, J.T.; Boerio, F.J. *Journal of Adhesion* **1994,** *46,* 243

5. Grunz, M. *Proceeding of the 16th Annual Meeting of The Adhesion Society,* The Adhesion Society, Inc.: Blacksburg, VA, **1993**, 378

6. Kwan, W.S.V.; Atanasoska, L.; Miller, L.L. *Langmuir* **1991,** *7,* 1419

7. Young, J.T.; Boerio, F.J.; Jackson, K.M. *Journal of Adhesion* **1994,** *44,* 103

8. Young, J.T.; Boerio, F.J. *Journal of Adhesion* **1994,** *44,* 119

9. Francis, S.A.; Ellison, A.H. *Journal of the Optical Society of America* **1959,** *49,* 131

10. Greenler, R.G.; Rahn, R.R.; Schwartz, J.P. *Journal of Catalysis* **1971,** *23,* 42

11. Greenler, R.G. *Journal of Chemical Physics* **1966**, *44*, 310

12. Greenler, R.G. *Journal of Chemical Physics* **1968**, *50*, 1963

13. McIntyre, J.D.E.; Aspnes, D.E. *Surface Science* **1971**, *24*, 417

14. Born, M.; Wolf, E. *Principles of Optics*, Pergamon Press Inc., New York, **1959**

15. Swalen, J.D.; Rabolt, J.F. *'Characterization of Orientation and Lateral Order in Thin Films by Fourier Transform Infrared Spectroscopy', in "Fourier Transform Infrared Spectroscopy: Applications to Chemical Systems",* eds Ferraro, J.R.; Basile L.J. Academic Press, New York, Chapt. 7, **1985,** *4,* 283

16. Bradshaw, A.M. *Applied Surface Science* **1982,** *11/12,* 712

17. Hoffmann, F.M. *Surface Science Reports* **1983,** *3,* 107

18. Golden, W.G..; *'Fourier Transform Infrared Reflection-Absorption Spectroscopy', in "Fourier Transform Infrared Spectroscopy: Applications to Chemical Systems",* eds Ferraro, J.R.; Basile L.J. Academic Press, New York, Chapt. 8, **1985,** *4,* 315

19. Adamson, A.W. *Physical Chemistry of Surfaces,* 5th ed.; John Wiley and Sons: New York, **1990**

20. Bard, A.J.; Faulkner, L.R. *Electrochemical Methods,* Wiley, New York **1980**

21. Imabayashi, S.; Iida, M.; Hobara, D.; Feng, Z.Q.; Niki, K.; Kakiuchi, T. *Journal of Electroanalytical Chemistry* **1997,** *428,* 33

22. Cavadas, F.; Anderson, M.R. *Langmuir* **2003,** *19,* 9724

23. Sabatani, E.; Rubinstein, I. *J. Phys. Chem.* **1987,** *91,* 6663

24. Finklea, H.O.; Snider, D.A.; Fedyk, J.; Sabatani, E.; Gafni, Y.; Rubinstein, I. *Langmuir* **1993,** *9,* 3660

25. Hayes, W.A.; Shannon, C. *Langmuir* **1996,** *12,* 3688

26. Batz, V.; Schneeweiss, M.A.; Kramer, D.; Hagenström, H.; Kolb, D.M.; Mandler, D. *Journal of Electroanalytical Chemistry* **2000,** *491,* 55

27. Young, J.T.; Boerio, F.J. *Langmuir* **1996,** *12,* 1219

28. Colthup, N.B.; Daly, L.H.; Wiberley, S.E. *Introduction to Infrared and Raman Spectroscopy* Academic Press, New York **1975**

29. Wilson, E.B.; *Phys. Rev.* **1934,** *45,* 706

30. Varsanyi, G. *Vibrational Spectra of Benzene Derivatives* Academic Press, New York **1974**

31. Osawa, M.; Matsuda, N.; Yoshii, K.; Uchida, I. *J. Phys. Chem.* **1994,** *98,* 12702

32. Hayes, W.A.; Shannon, C. *Langmuir* **1996,** *12,* 3688

33. Orszagh, J.Z.; Orzeszko, A.; Chreptowicz, T. *Eur. Polym. J.* **1979,** *16,* 289

34. Sauers, C.K.; Gould, C.L.; Ioannou, E.S. *J. Am. Chem. Soc.* **1972,** *94,* 8156

35. Sauers, C.K. *J. Org. Chem.* **1969,** *34,* 2275

36. Orzeszko, A.; Banbula, W.K. *Eur. Polym. J.* **1991,** *27,* 1107

37. Hayes, W.A.; Shannon, C. *Langmuir* **1996,** *12,* 3688

Chapter 4

Impedance Spectroscopy of Aromatic Thiol Self-Assembled Monolayers on Gold Substrate: Influence of Different Electrolytes, Solution Concentration, Self-assembling Time, Applied Potential, and Molecular Structure

4.1 Introduction

Electrochemical impedance spectroscopy (EIS) is a very powerful method for studying corrosion[1,2,3,4,5,6,7,8,9,10] and characterizing modified electrodes[11,12,13]. Some of the advantages of EIS techniques over other techniques are:

1. the use of low-amplitude sinusoidal voltage (about 5 mV) which makes the system only marginally perturbed from equilibrium (steady state),
2. the possibility of obtaining information on important quantities such as ohmnic resistance, double layer capacitance, capacitance of the film, as well as about other important processes such as charge transfer at the electrode/film interface and within the film in a single experiment,
3. the possibility of characterizing interfacial properties in the absence of a redox reaction.

Theoretically, a SAM prepared with an ideal dielectric material and no current leakage at defect sites obeys the Helmholtz ideal capacitor model (parallel plate capacitor with a dielectric material)[14,15]. The gold surface acts as one capacitor plate and the physisorbed ions at the SAM/electrolyte interface act as the other capacitor plate. The

backbone of SAM is the intervening dielectric material. EIS is able to test the Hemholtz model with SAM-modified electrodes by using an appropriate equivalent circuit.

In the analysis, a small-amplitude sinusoidal signal is applied to the electrochemical cell and the current response is monitored under potentiostatic control. For a given applied potential, $V(t) = V_0 \cos(\omega t)$, the resulting steady state current is given by $I(t) = I_0 \cos(\omega t-\theta)$. Here θ is the phase shift between the voltage and the current. This phase shift will be a function of the frequency of the input voltage. The relationship between the voltage applied across a typical resistor and a capacitor circuit at a given frequency is schematically illustrated in figure 4.1. The impedance can be expressed as a complex number $Z(\omega) = V(t)/I(t) = Z_0 (\cos\theta + j\sin\theta) = Z'(\omega) + jZ''(\omega)$, which is frequency-dependent. Z' is the real component of the impedance for the electrochemical cell and Z" is the imaginary component of the impedance. A common way to graphically present impedance data for a given system is plotting –Z" against Z'. This data presentation is commonly called the Nyquist plot. Each point on the Nyquist plot is characteristic of the complex impedance at a given frequency; however, this data representation does not indicate what the frequency is. Another data presentation method is the "Bode plot". In a Bode plot, the impedance is plotted against the log(frequency) and both the absolute value of the impedance ($|Z| = Z_0$) and the phase-shift are plotted on the y-axis. Unlike the Nyquist plot, the Bode plot explicitly shows frequency information. The phase shift can also provide information about the cell time constants and the ideality of the SAMs capacitive behaviour. Figure 4.2 and 4.3 are Nyquist plot and Bode phase plot of a simplified Randles Cell. This simplified Randles cell is the equivalent circuit used to fit our impedance data.

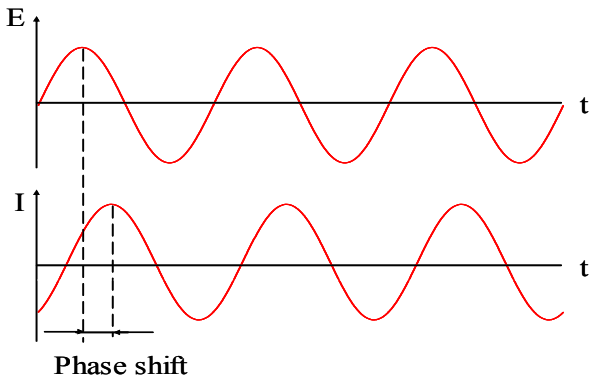

Figure 4.1. Phasor diagram for voltage and current.

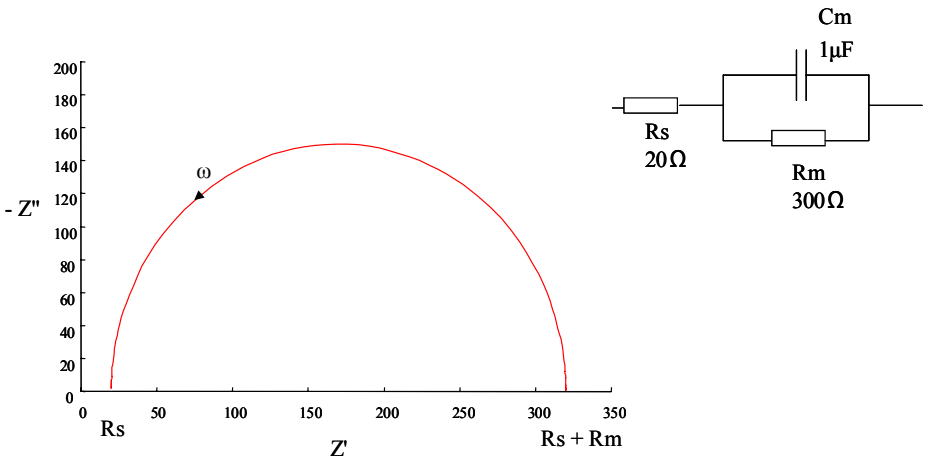

Figure 4.2. Nyquist plot of a simplified Randles cell. Low frequency data are on the right side of the plot and higher frequencies are on the left. This is true for EIS data where impedance usually falls as frequency rises (this is not true of all circuits).

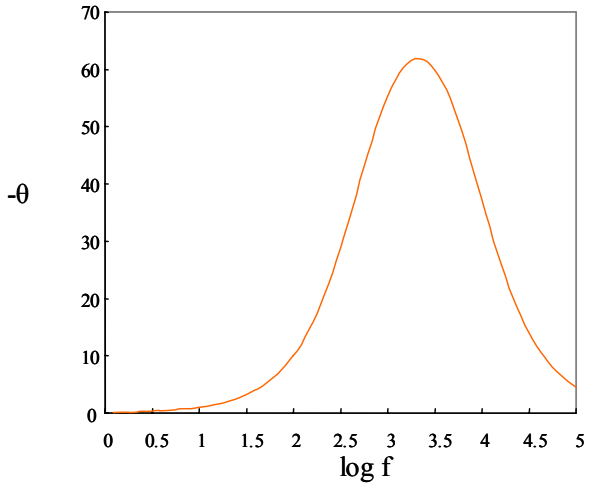

Figure 4.3. Bode phase plot of a simplified Randles cell.

It should be noted that electrochemical interfacial systems are only approximately modeled by the idealized circuit elements over a limited range of experimental conditions. All real elements extend over a finite region of space rather than being localized at a point and have distributed behavior. Although ideal resistors and capacitors are usually used in the experimental fit, an electrochemical cell is always finite in some extent and exhibits different types of distributed response. A constant phase element (CPE) is one commonly used distributed element and will be used here to fit our impedance data. Mathematically, a CPE's impedance is given by equation (4-1),

$$Z_{CPE} = A (j\omega)^{-\alpha} \qquad (4\text{-}1)$$

This equation describes an ideal capacitor for $\alpha = 1$ and an ideal resistor for $\alpha = 0$[16]. The CPE is explicitly described by Cole and Cole[17]. Many publications emphasize the importance and ubiquity of the CPE in fitting electrochemical data to a theoretical circuit[16]. Several theories have been proposed to account for the non-ideal behavior of the double layer, but none has been universally accepted. Some possible explanations are

electrode surface roughness, inhomogeneous reaction rates on a surface, or varying thickness or composition of a coating.

In this technique, the impedance of an electrochemical cell over a wide range of frequencies was determined and then an equivalent circuit was used to quantitatively describe the impedance as a function of frequency. The direct connection that often exists between the behavior of a real system and that of an idealized model circuit consisting of discrete electrical components is one of the most attractive aspects of impedance spectroscopy as a tool for investigating the electrochemical properties of systems. The ambiguity of the model chosen is one of the problems of EIS. Equivalent circuits are seldom unique and only the simplest circuits can be said to be unambiguous in their description of experimental data. Some criteria applied to choose a model of an equivalent circuit to fit EIS data are: (1) the model should be appropriate to the physical description of the given system; (2) the model should be as simple as possible and contain as few adjustable parameters as possible; (3) additional experimental techniques should be applied to confirm the model when they are available; (4) statistical tools should be used to determine the relative importance of each element in the equivalent circuit.

The best method of quantitative analysis of impedance data is fitting the data to a theoretical model and/or equivalent electrical circuit by using Complex Nonlinear Least Squares (CNLS) fitting. MacDonald and Garber first applied it to their EIS work[16,18,19]. Here, CNLS fitting was performed using LEVM software version 8.0. The quality of the overall fitting was determined by the relative standard deviation of parameters. The criteria that a free parameter or a circuit element should be removed from the equivalent circuit when the relative standard deviation of the parameter is on the order of 30% or

more. The best set of parameters is defined as that minimizes the sum S_m:

$$S_m = \sum \omega_j^{'}(X_e^{'} - X_{th}^{'})_j^2 + \omega_j^{''}(X_e^{''} - X_{th}^{''})_j^2 \qquad (4\text{-}2)$$

Where *m* is the total number of data points. X' and X" are the real part and the imaginary part of the immittance of the j^{th} point, respectively. Subscripts "e" and "th" denote the experimental values and values calculated from the equivalent circuit.

In this chapter, the effect of electrolyte, the concentration of electrolyte solution, the deposition time, and the potential on the ionic insulating properties of aromatic thiol SAMs were tested by electrochemical impedance spectroscopy. The ionic insulating properties of aromatic thiol SAMs are addressed here in the absence of redox-active species.

4.2 Experimental

EIS measurements were conducted on SAM modified gold substrates in the frequency range from 10 KHz to 1 Hz. Data points were collected at intervals spaced on a logarithmic scale, 12 points per decade, under excitation of a sinusoidal wave of 10 mV amplitude. Self-assembling time of aromatic thiols on the gold substrate depends on the experimental requirements. The electrochemical cell described in chapter 2 was used here. In all impedance spectra presented here, symbols represent the experimental raw data, and the solid lines are the fitting curves obtained from CNLS data fits. Data is presented Nyquist plots and Bode phase plot here.

4.3. Results and Discussion

4.3.1. Establishing Equivalent Circuit

Many types of equivalent circuit models have been proposed and used in the literature to interpret impedance behavior of the SAMs covered electrodes[20,21,22,23]. The equivalent circuit shown in figure 4.4 best models our EIS data. It consists of a solution resistance (R_s) in series with a parallel network of a constant phase elements (CPE) and SAM resistance (R_{sam}). The Bode phase plot indicated that the ATP and MPP SAMs investigated here behaved as a capacitor with leakage at the defect sites, and it is sufficient to include a resistance in parallel to SAM capacitance in the model to account for the penetration of ions and/or water into the body of the SAM. Thus, R_{sam} in the equivalent circuit represents the ionic conductivity of the SAM.

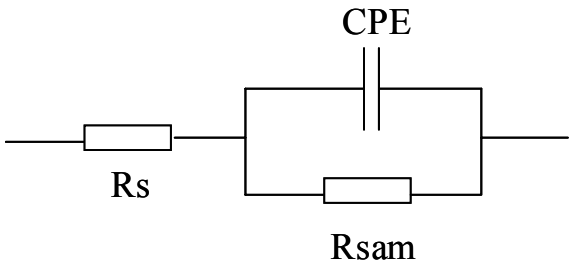

Figure 4.4. Schematic of equivalent circuits used in this analysis. The model describes a SAM with defects on the gold surface in the case that Z_w is ignored and $R_{sam} \gg R_t$. Rs is the solution resistance, Rsam is the resistance of SAM and accounts for the permeability of ions and/or water within the SAM, and CPE represents the capacitance of SAM.

4.3.2. Influence of Different Electrolytes

3-ATP SAMs were first analyzed by EIS at a benign dc potential (i.e., nonaltering to the SAM)[22] in 50 mM KCl, KClO4, and Na2HPO4 electrolyte solutions. Theoretically, a 90° phase angle means that the SAM obeys the Helmholtz ideal capacitor model. In this case, no current leakage occurs at defect sites and the SAM is an ideal dielectric material[16]. Practically, the total impedance is dominated by the solution resistance at high frequency. In the low-to-medium frequency range (1 Hz ‹ f ‹ 10^3 Hz), a SAM behaves like a pure capacitor when its phase angle is higher than 88°, while a SAM whose phase angle is lower than 87° is viewed as a capacitor contaminated by a resistive component with current leakage at defect sites. The phase angle at 1 Hz frequency is suitable for evaluation provided that diffusion-related phenomena occur in this time domain[24]. Phase angles of 3-ATP/Au SAM in three electrolytes at 1 Hz are all lower than 88°, indicating that all ions can penetrate into the body of SAM on the defect sites. Among three electrolytes, Na_2HPO_4 has the highest impedance and also highest phase angle at 1 Hz. Na_2HPO_4 was chosen as the electrolyte for all other EIS experiments discussed in this chapter. Na_2HPO_4 has more charge and a bigger size than KCl and $KClO_4$; however, KCl, which has the same charge but smaller size than $KClO_4$, has a higher impedance. The relationship between the charge and the size of ions and their permeability to the SAM was not investigated systematically here.

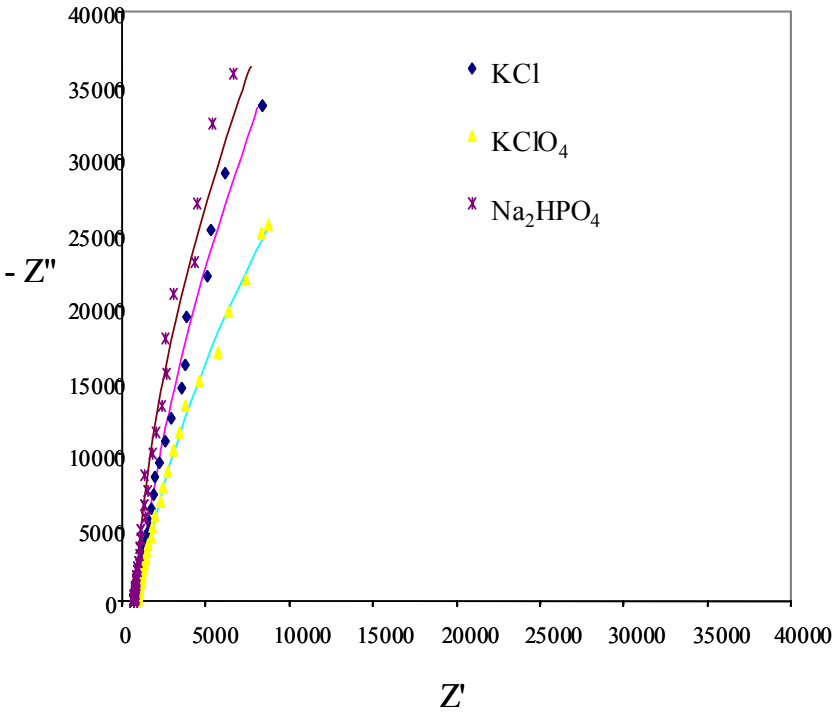

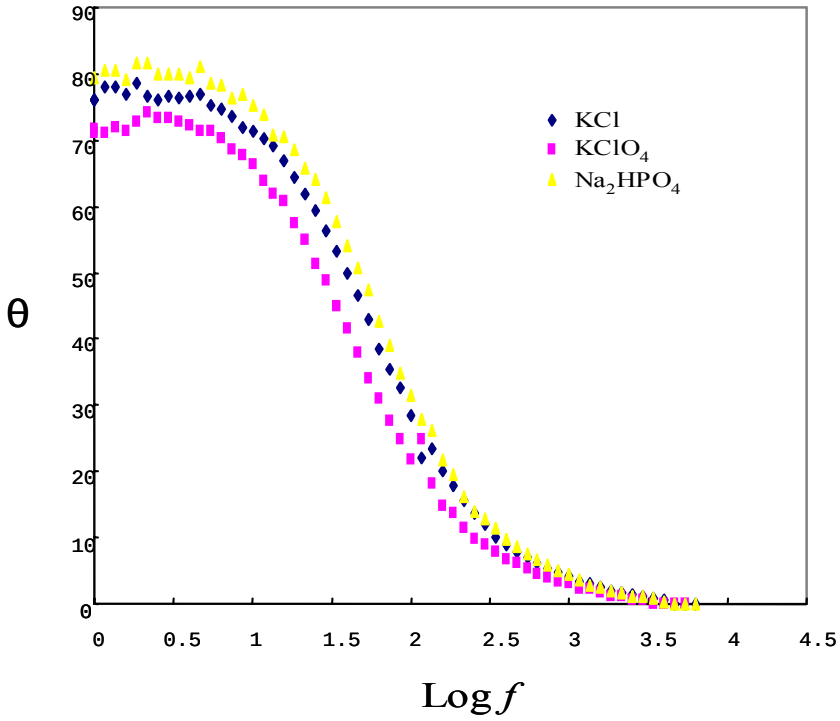

Figure 4.5. Nyquist plots and Bode phase plot of 3-ATP/Au SAMs at different electrolyte. Impedance spectra were acquired at 0.2 V vs Ag/AgCl in 50 mM electrolyte solution.

4.3.3.Influence of Electrolyte Concentrations

Figure 4.6 shows the Nyquist plot of 3-MPP/Au SAMs in aqueous Na_2HPO_4 solution at four different electrolyte concentrations. The phase angles at 1 Hz for 3-MPP/Au SAMs were lower than 88° from 2 mM to 50 mM. Again, 3-MPP/Au SAM did not behave like a pure capacitor, and the impedance data were fit using the equivalent circuit described in figure 4.4. The fitting parameters are given in Table 4.1. As expected, the solution resistance decreased linearly with the electrolyte concentration[25].

For a defect-free SAM, the ions in the electrolyte solution were blocked on the SAM/electrolyte interface and the SAM capacitance values should not change significantly with the electrolyte concentration. The 3-MPP/Au SAM capacitance values reported here ranged from 4.08 μF at 2 mM to 4.36μF at 50 mM, as shown in figure 4.7. The increasing of the SAM capacitance with the electrolyte concentration was due to the ion permeation into the body of the SAM. In the higher concentration solution, more ions penetrated into the SAM. This had the same effect as decreasing the distance between two capacitor plates and causing the increase in the capacitance. This further demonstrated that these SAMs were not defect-free.

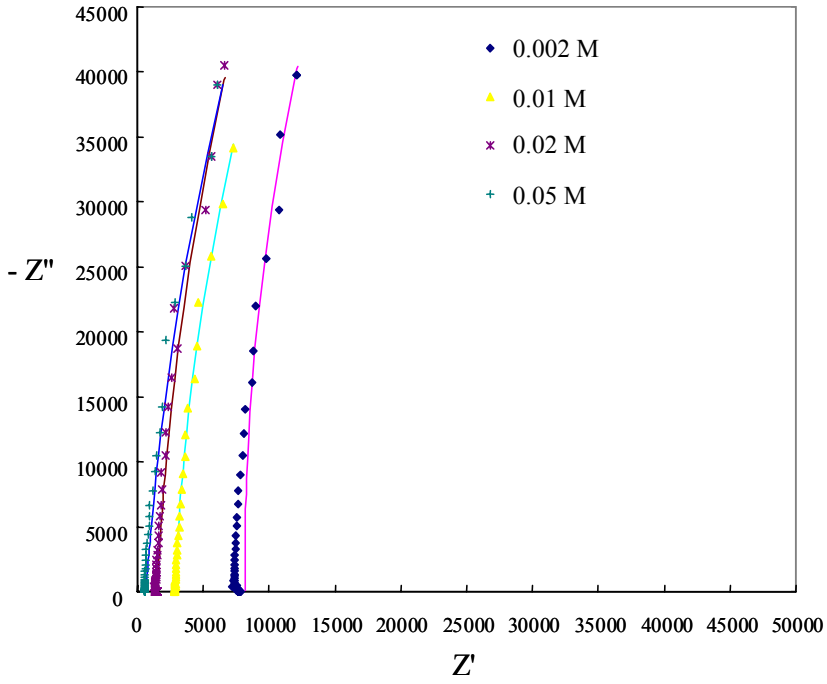

Figure 4.6. Nyquist plot of 3-MPP/Au SAMs at various electrolyte concentrations. Impedance spectra were obtained at 0.2 V vs Ag/AgCl in Na_2HPO_4 at various concentrations.

Table 4.1. CNLS Fitting Parameters for 3-MPP/Au SAMs as a Function of Electrolyte Concentration

Concentration(mM)	Rs($10^2\Omega$)	R_{sam}($10^5\Omega$)	CPE(μF)	α
2	74.23±0.30	4.81±0.32	4.08±0.03	0.98±0.003
10	28.64±0.11	3.83±0.13	4.09±0.02	0.98±0.002
20	10.56±0.15	4.93±0.29	4.12±0.02	0.97±0.002
50	6.47±0.18	4.96±0.29	4.34±0.02	0.96±0.002

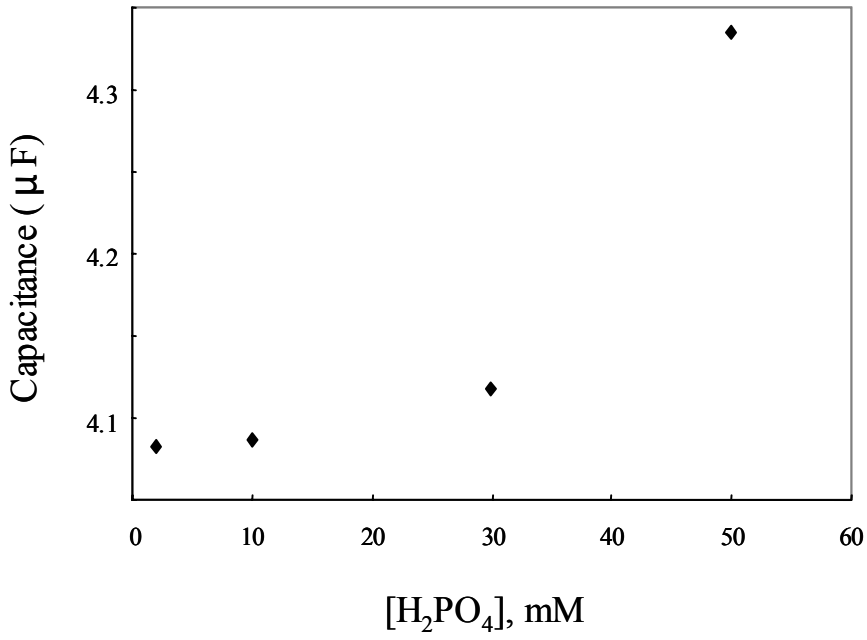

Figure 4.7. Plot of 3-MPP/Au SAM capacitance against electrolyte concentration at 0.2 V vs Ag/AgCl.

4.3.4. Influence of Various Self-assembling Time

The growth of thiols on gold substrate was reported to have two processes. A fast process in which a disordered monolayer is deposited in a few seconds for milimolar to higher concentrations is followed by a much slower process in which a highly oriented and densely packed monolayer is formed over a period of hours to days. Here the change in the phase angle and the SAM capacitance of a 3-ATP/Au SAM were monitored after various self-assembling time of a freshly prepared gold slide in the thiol solution to follow the formation of aromatic SAMs on the gold substrate. The EIS experiments were run ex situ at 0.2 V vs Ag/AgCl in 50 mM Na_2HPO_4 solution.

As observed in figure 4.8, the impedance and the phase angle in the low-frequency range increased dramatically as the self-assembling times increased. The phase

angle at 1 Hz never achieved 88°. A maximum phase angle of 80 at 1 Hz was achieved after 48 hours of self-assembling in the thiol solution, and a longer self-assembling time did not increase the phase angle at 1 Hz. The phase angle at 1 Hz changed from 48° to 80° between 30 minutes and 48 hours, which is increased by 67%.

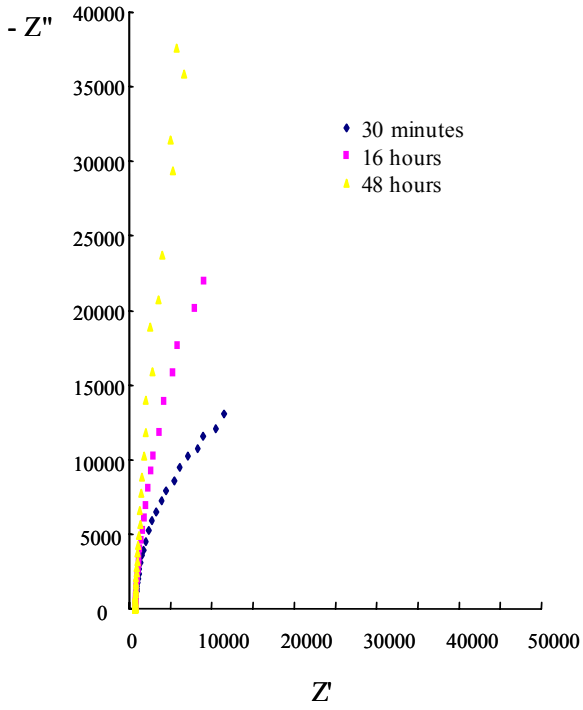

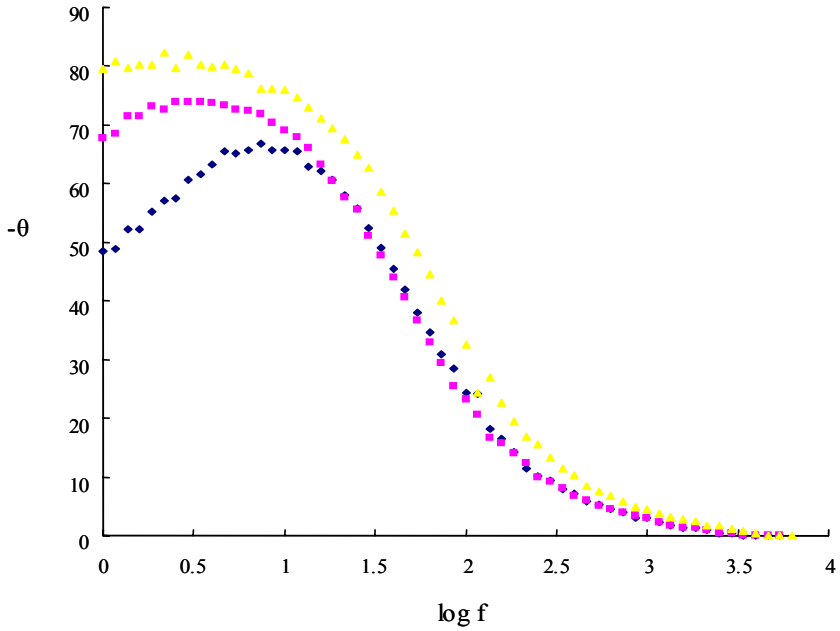

Figure 4.8. Nyquist and Bode phase plot of a 3-ATP/Au SAM acquired after various self-assembling times in the thiol solution. The impedance spectra were run ex situ at 0.2 V vs Ag/AgCl in 50 mM Na_2HPO_4 solution.

Data were fit by using the equivalent circuit shown in figure 4.4. Table 4.2 gives the fitting parameters. The resistance of the SAM increased from 35 KΩ to 300 KΩ, while the capacitance of SAM decreased from 8.92 μF to 4.58 μF between 30 minutes and 48 hours. These results indicated that when the time the gold substrate was incubated in the thiol solution increased, a more densely packed SAM was formed on the gold surface and ions were blocked from approaching the gold surface.

Table 4.2. CNLS Fitting Parameters for 3-ATP/Au SAMs as a Function of Self-Assembling Time

Time(h)	Rs($10^2\Omega$)	R_{sam}($10^5\Omega$)	CPE(μF)	α
0.5	6.42±0.29	0.352±0.009	8.92±0.17	0.858±0.007
16	7.45±0.15	0.98±0.02	7.09±0.05	0.928±0.003
48	7.34±0.27	3.07±0.26	5.88±0.06	0.944±0.004

4.3.5 Influence of Applied Potential

Boubour and Lennox investigated the ionic permeability of *n*-alkanethiol SAMs and *ω*-functionalized SAMs chemisorbed on gold using EIS in the absence of redox active species as a function of applied potentials[22,25]. The behavior of the phase angle at frequencies of less than about 50 Hz revealed that all these alkanethiol SAMs were ionic insulators and could be well described by the Helmholtz capacitor model until a critical potential, V_c, was reached or exceeded. Once the applied potentials were more cathodic than V_c, they all behaved like leaky capacitors and significant changes in the phase angle at 1 Hz associated with ion penetration was observed. Ion penetration into the alkanethiol SAMs were activated at this critical potential. V_c was dependent on both the chain length and the chemical nature of the terminal groups.

The effect of the applied potential on a 4-MPP/Au SAM permeability is shown in Figure 4.9 and 4.10. The applied potential was varied from + 0.4 V to – 0.7 V in 0.1 V steps. The impedance spectra were superimposable upon one another when the applied potential was changed from – 0.2 V to 0.4 V (vs Ag/AgCl). The phase angle at low

frequency domain is lower than 88°, and the experimental data were fitted using the equivalent circuit of leaking capacitor shown in figure 4.4. In this case, no transformation of SAMs from being ionic insulators to being leaky capacitors occurred, so no critical potential was defined here.

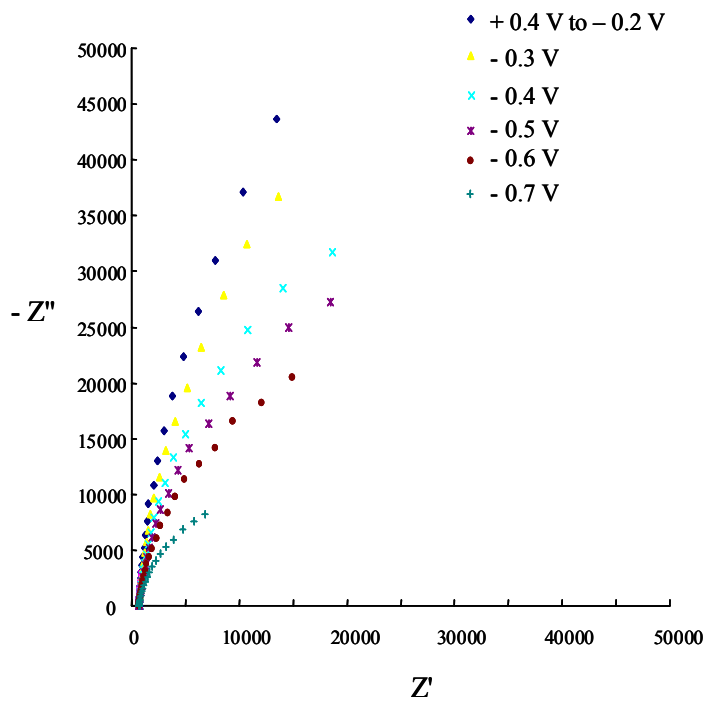

Figure 4.9. Nyquist plot of a 4-MPP/Au SAM at different applied potentials. Impedance spectra were acquired in 50 mM Na_2HPO_4 solution.

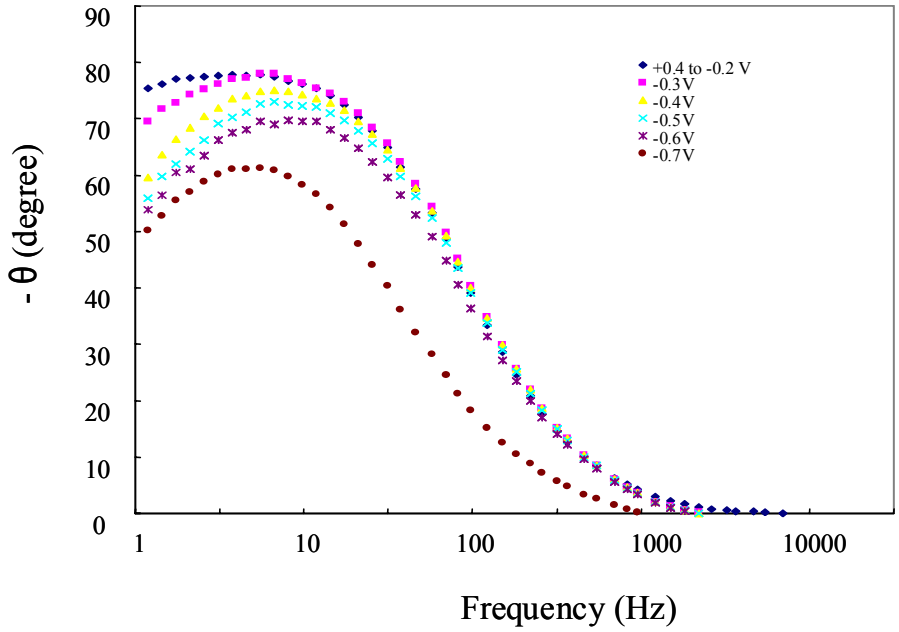

Figure 4.10. Bode phase plot of a 4-MPP/Au SAM at different applied potentials. Impedance spectra were acquired in 50 mM Na_2HPO_4 solution.

Although the 4-MPP/Au SAMs were not defect-free, the increasingly cathodic applied potential induced more defects in the SAM. At -0.3 V and beyond, the impedance became smaller and the phase angle in the low frequency domain deviated from the highest 76° with more cathodic applied potentials. However, the deviation from the highest impedance and phase angle here was more gradual than that of alkanethiol SAMs. Another predominant difference is that the phase angle decreased not only in the low frequency domain but also in the medium to high frequency domain. When the applied potential was – 0.4 V and beyond, the phase angle no longer reached to the 80° in the medium frequency domain. Boubour and Lennox concluded that when the applied potential exceeded the critical potential, the electric field facilitated ion penetration by lowering the energy barrier in the SAM itself. Rigid aromatic thiol molecules are bigger

than alkanethiols and the aromatic thiol SAM surface coverage is much smaller than that of alkanethiol SAM. This might be the reason that ions can penetrate into the aromatic thiol SAMs more easily and they are not good ionic insulators. However, the lateral interaction within aromatic thiol SAMs should be stronger than that of alkanethiol SAMs because of the strong π-π interactions and lowering the energy barrier by increasing the applied potential more cathodic should be more difficult in the aromatic thiol SAMs than in the alkanethiol SAMs.

4.3.6 Influence of Molecular Structure on Passivation Properties of SAMs

Above studies optimized conditions to make electrochemical impedance spectroscopy measurements on gold substrates: 50 mM Na_2HPO_4 solution, applied potential of 0.2 V. When we looked into the molecular structures of 3-ATP, 4-ATP, 3-MPP, and 4-MPP SAMs, we noticed that 3- and 4-ATP SAMs have hydrophilic amino tail groups, while 3- and 4-MPP have hydrophobic imide tail groups; and 3-ATP and 3-MPP SAMs have their tail groups substituted at different position than 4-ATP and 4-MPP SAMs, respectively. Impedance of these four SAMs on gold substrates was measured to address the influence of molecular structure on the passivation properties of SAMs on gold substrates. As discussed previously, R_{sam} in the equivalent circuit represents the ionic conductivity of the SAM and are used to evaluate the passivation properties of SAMs here.

Table 4.3 showed the fitting parameters for the above four self-assembled monolayer systems. The 4-MPP monolayer was found to have the highest monolayer resistance to ion transport. Other three SAMs showed similar but significantly poorer

inonic insulating properties than 4-MPP SAM. This result suggested that 4-MPP formed the most densely packed monolayer on the gold substrates. More investigations were done on these four SAMs systems to get a better understanding on their passivation properties.

Table 4.3. CNLS Fitting Parameters for 3-ATP, 4-ATP, 3-MPP, and 4-MPP SAMs on gold substrates

SAM	$R_s(10^2\Omega)$	$R_{sam}(10^5\Omega)$	$C_{sam}(\mu F)$
3-ATP	7.34±0.27	3.07±0.26	5.88±0.06
3-MPP	6.47±0.18	4.96±0.29	4.34±0.02
4-ATP	6.82±0.13	4.06±0.30	6.64±0.04
4-MPP	6.99±0.37	9.41±1.06	2.91±0.02

Contact angle measurement results discussed in chapter 3 revealed that 4-MPP had the highest contact angle and was the most hydrophobic among them. Ions in the aqueous electrolyte solution should be repelled farthest away from the gold surface in this case.

In reductive desorption measurements, Au-SR bond is cleaved and reduced to RS^-. The potential of reductive desorption peak is affected by the lateral interactions in the SAM. The additional stabilizing lateral interactions in the SAM moves the reductive desorption peak potential more negative. Surface coverage of SAMs can be calculated by integrating the reductive desorption peak area. All four monolayers exhibit reductive desorption peaks. The reductive desorption peak potential and surface coverage of each

SAM are summarized in table 4.4. No big difference in the surface coverage was observed for all four SAMs. However, the reductive desorption peak potential of 4-MPP SAMs was the most negative. These results indicated that although the surface coverage of 4-MPP SAMs was not significantly higher than the other three, it had the strongest lateral interactions among them all. The best passivation property of 4-MPP SAMs on gold surface may be accounted to the hydrophobility of the SAM and the strong lateral interactions within the SAMs.

Table 4.4. Reductive desorption potential and surface coverage results for 3- and 4-ATP, 3-and 4-MPP monolayers on gold substrates

Monolayer	Potential (V)	Surface Coverage (10^{-10} mol/cm^2)
4-ATP	-0.724	3.56±0.06
4-MPP	-0.802	4.1±0.1
3-ATP	-0.678	3.6±0.1
3-MPP	-0.684	3.3±0.2

4.4. Conclusions

Impedance spectra of self-assembled monolayers on gold substrates were tested for the optimum measurement condition. Na_2HPO_4 is the optimal electrolyte because it has the highest impedance and also highest phase angle at 1 Hz among the three tested electrolytes. Solution resistance decreased when the electrolyte solution concentration increased. 0.05 M Na_2HPO_4 was used as the optimal electrolyte concentration.

Impedance spectra for various self-assembling time confirms two phases in the self-assembling process. Impedance of self-assembled monolayers is constant when applied potential is more anodic than certain potential while defects are introduced at more cathodic potentials. Defects were induced in the monolayer at DC potentials more cathodic than -300 mv for 4-MPP SAM. So the applied potential of 200 mv was used in the experiments. In conclusion, 0.05 M Na_2HPO_4 solution at 200 mV applied DC potential is the optimum condition for the impedance spectroscopy measurements. Impedance data for 3-ATP, 4-ATP, 3-MPP, and 4-MPP SAMs on gold substrates showed the highest R_{sam} value for 4-MPP SAMs. 4-MPP SAM is most hydrophobic among them, and has the strongest intermolecular interactions might be the reason it has the highest resistance to ion transport.

4.5 Reference

1. Deflorian, F.; Fedrizzi, L.; Bonora, P. L. *Prog. Org. Coat.* **1993,** *23,* 73

2. Deflorian, F.; Miskovic-Stankovic, V. B.; Bonora, P. L.; Fedrizzi, L. *Corrosion* **1994,** *50,* 438

3. Kendig, M.; Scully, J. *Corrosion* **1990,** *46,* 22

4. Mansfeld, F.; Chen, C.; Lee, C. C.; Xiao, H. *Corros. Sci.* **1996,** *38,* 497

5. Bonora, P. L.; Deflorian, F.; Fedrizzi, L. *Electrochim. Acta* **1996,** *41,* 1073

6. Griffin, A. J. J.; Brotzen, F. R. *J. Electrochem. Soc.* **1994,** *141,* 3473

7. Su, P.-C.; Devereux, O. F. *Corrosion* **1998,** *54,* 419

8. Mertens, S. F.; Xhoffer, C.; DeCooman, B. C.; Temmerman, E. *Corrosion* **1997,** *53,* 381

9. Scholl, H.; Jimenez, M. M. D. *Corros. Sci.* **1992,** *33,* 1967

10. Lin, S.; Shih, H.; Mansfeld, F. *Corros. Sci.* **1992,** *33,* 1967

11. Lang, G.; Bacskai, J.; Inzelt, G. *Electrochim. Acta* **1993,** *38,* 773

12. Tsai, C. H.; Mansfeld, F. *Corros. Sci.* **1993,** *49,* 726

13. Mansfeld, F.; Kendig, M. W.; Tsai, S. *Corrosion* **1982,** *38*, 478

14. Helmholtz, H. *Ann. Phys.* **1879,** *7,* 337

15. Halliday, D.; Resnick, R. *Physics,* Wiley: New York, ***1978***

16. Macdonald, R. J. *Impedance Spectroscopy: Emphasizing Solid Materials and Systems;* 1 ed.; John Wiley and Sons: Chapel Hill, NC, **1987**

17. Cole, K. S.; Cole, R. H. *Journal of Chemical Physics* **1941,** *9,* 341

18. Macdonald, R. J.; Garber, J. A. *Journal of the Electrochemical Society* **1977,** *124,* 1022

19. Macdonal, R. J.; Schoonman, J.; Lehnen, A. P. *J. Electroanal. Chem.* **1982,** *131,* 77

20. Jennings, G. K.; Munro, J. C.; Yong, T. –H.; Laibinis, P. E. *Langmuir* **1998,** *14,* 6130

21. Protsailo, L. V.; Fawcett, W. R. *Langmuir* **2002,** *18,* 8933

22. Boubour, E.; Lennox, R. B. *Langmuir* **2000,** *16,* 4222

23. Janek, R. P.; Fawcett, W. R.; Ulman, A. *Langmuir* **1998,** *14,* 3011

24. Janek, R. P.; Fawcett, W. R.; Ulman, A. *J. Phys. Chem. B* **1997,** *101,* 8550

25. Boubour, E.; Lennox, R. B. *J. Phys. Chem.* **2000,** *104,* 9004

Chaper 5

Electrochemical Investigation of 3- and 4-MPP Self-assembled Monolayers to Inhibit Copper Corrosion

5.1 Introduction

After studying the properties of 3- and 4-MPP SAMs on gold substrates, we characterized the interface properties of copper substrates modified with 3-MPP and 4-MPP in the place of corrosive solutions using electrochemical methods.

Copper is widely used in the chemical process industries, and for microelectronics applications due to its high thermal and electrical conductivities and low cost. Compared to gold, copper is more reactive, is more difficult to clean and handle, and is spontaneously oxidized. These are properties limited the use of copper. Like thiol-Au systems, self-assembled monolayers can be formed on copper surfaces by the chemisorption of *n*-alkanethiols [$CH_3(CH_2)_{n-1}SH$]. As reviewed in the Chapter 1, the formation of densely packed and crystalline *n*-alkanethiol self-assembled monolayers onto copper provides a convenient system to protect the underlying metal surface from corrosion and oxidation[1,2,3,4,5,6,7,8]. Other protective films, such as two-dimensional polymers[9,10,11,12,13,14], sodium S-alkyl thiosulfates SAMs[15], Schiff bases SAMs[16,17,18], also provided efficient corrosion protection on copper. Self-assembled monolayers of aromatic thiols have not been studied as corrosion inhibitors on copper to our knowledge. In this chapter, we investigated the corrosion protection properties of 3- and 4-MPP SAMs on copper surfaces to address the effect of substitution patterns of benzene rings on the protection efficiency of SAMs. The

protection efficiency was determined by electrochemical impedance spectroscopy and polarization measurements.

Corrosion takes place when a metal surface reacts with its environment. In an aqueous environment and in an atmospheric environment which also involves thin aqueous layers, corrosion is largely an electrochemical process because of the transfer of electrons between a metal surface and an aqueous electrolyte solution involved in corrosion. The same metallic surface exposed to an aqueous electrolyte usually possesses anodic and cathodic sites that make up a corrosion cell. The process occurring at the anodic sites is the dissolution of metal such as

$$M \longrightarrow M^{n+} + n\,e^{-}$$

where M is a metal atom, and n is the number of electrons lost during anodic oxidation. The anodic reaction forms either soluble ionic products or an insoluble compound of the metal, such as an oxide, a hydroxide. This is the destructive process called corrosion. The liberated electrons travel through the bulk metal or another low resistance electrical connection to the cathode, where they are consumed by cathodic reactions. Several cathodic reactions are possible depending on what reducible species are present in the solution. Typical reactions are the reduction of dissolved oxygen gas, or the reduction of the solvent (water) to produce hydrogen gas. The corrosion current formed by the flow of electrons between the corroding anodes and the non-corroding cathodes is determined by the rate of production of electrons by the anodic reaction and their consumption by the cathodic reaction.

Each oxidation or reduction reaction has associated with it a potential determined by the tendency for the reaction to take place spontaneously. The difference in potential between the anodic and cathodic sites is the driving force for electrons to flow between the

anodes and the cathodes. The potential is a measure of the corrosion tendency. However, the determination of the corrosion tendencies by measuring potentials is not sufficient to ascertain whether a given metal or alloy will suffer corrosion under a given set of environmental conditions because the rate of corrosion may be very low and corrosion may not be a problem even though the tendency for corrosion may be high.

Corrosion rates are determined by applying a current to produce a polarization curve, which shows the degree of potential change as a function of the amount of current applied, for the metal surface whose corrosion rate is being determined. The application of the current in a positive direction signifies that the metal surface is anodically polarized, while a negative direction signifies that it is cathodically polarized. How the rates of the anodic and the cathodic reactions are retarded by various environmental and/or surface process factors is measured by the degree of polarization. The various environmental factors such as concentration of metal ions, dissolved oxygen, etc. in solution is called concentration polarization, and the surface process factors such as adsorption, film formation, ease of release of electrons, etc. is called activation polarization. The polarization curve allows one to study the effect of concentration and activation processes on the rate at which anodic or cathodic reactions can give up or accept electrons. Hence, polarization measurements can thereby determine the rate of the reactions that are involved in the corrosion process – the corrosion rate.

Figure 5.1 shows anodic and cathodic polarization curves that represent anodic reactions (like metal dissolution) or cathodic reactions (for example, oxygen reduction or hydrogen evolution). In Figure 5.1 the potential "E" is plotted as a function of the logarithm of the current density "i". A straight line on this plot following the Tafel equation (equation

5.1) suggests that the corrosion reactions are controlled by activation polarization, as is frequently observed.

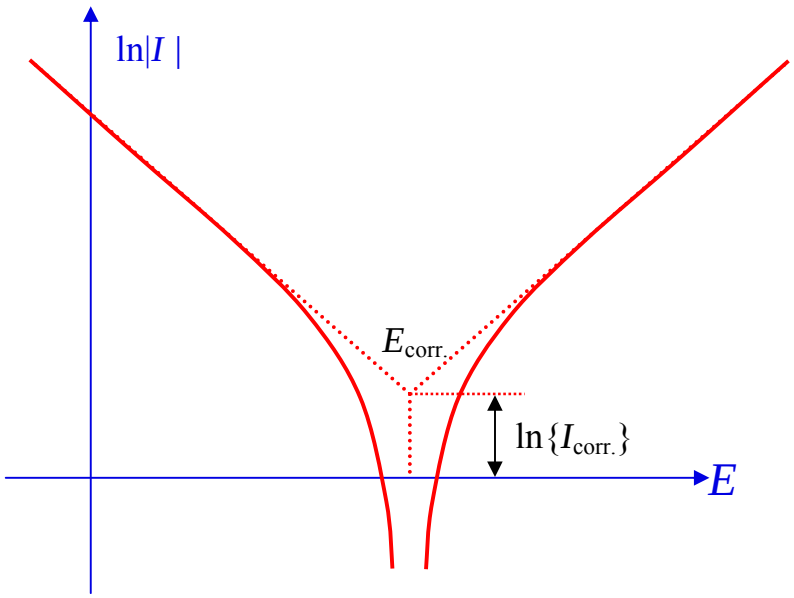

Figure 5.1. Schematic illustration of polarization curve (Tafel plot). The extroplations of the anodic and cathodic Tafel line intersect at the corrosion potential, E_{corr}. The value of the current at their intersection, i_{corr}, is the rate of corrosion expressed in current density.

The Tafel equation is an early (1905) empirical relation between the overpotential of the electrode and the current density passing through the electrode:

$$\eta = a + b \times \log i \qquad (5.1)$$

where η is the overpotential and i is the current density. "a" and "b" are characteristic constants of the electrode system. A polarization curve is also called the "Tafel plot" and the

resulting straight line the "Tafel line". Under ideal conditions, the extrapolations of the anodic and cathodic linear portions of the polarization curves intersect at the corrosion potential, Ecorr. The value of the current at their intersection will be the rate of corrosion "i_{corr}" expressed in current density.

In this chapter, electrochemical impedance spectroscopy and polarization curves were measured on both bare copper electrode and 3- and 4-MPP SAMs modified copper electrode in NaCl solution at room temperature. The protection efficiency of SAMs on copper corrosion was calculated in both measurements.

5.2 Results and Discussion

5.2.1 Electrochemical Impedance Spectroscopy

Figure 5.2 shows the Nyquist impedance plot of the unmodified copper electrode and a 4-MPP SAMs modified copper electrode in 0.2 M NaCl solutions. 4-MPP SAMs were formed by immersing the copper electrode in a 2 mM 4-MPP/ acetone solution with various self-assembling time, indicated on the plot.

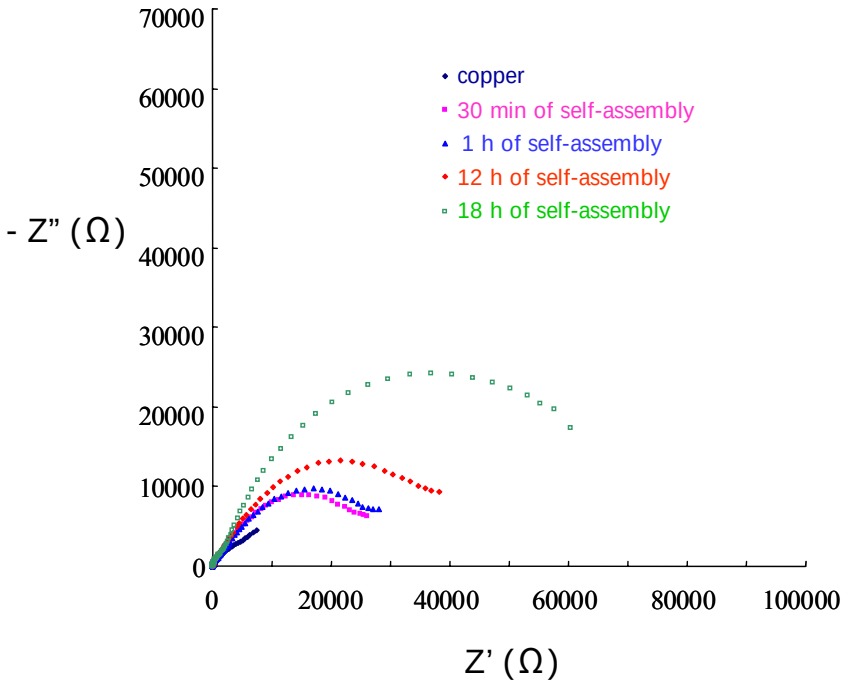

Figure 5.2. Nyquist impedance spectra for the uncovered and 4-MPP SAMs covered copper electrode with various self-assembly time in 2 mM thiol acetone solutions. Impedance spectra were acquired at the open-circuit potentials (vs. Ag/AgCl) in 0.2 M NaCl solutions.

The Nyquist plot for unmodified copper measured in 0.2 M NaCl solution showed a capacitive loop in the high frequency range. This capacitive loop is characteristic of the relaxation time constant of a charge-transfer resistance (R_t) whose value is approximately equal to the diameter of the capacitive loop and a double-layer capacitive (C_{dl}) at the copper/electrolyte interface[6,19,20,21]. The value of R_t retrieved from fitting parameters was 1.51×10^4 Ω using LEVMWL software. The easier the copper is corroded in a corrosive solution, the smaller the charge transfer resistance, R_t, is. Our result is in agreement with what reported in the literature[8]. In the NaCl solution, the corrosion at the copper surface was due to the anodic dissolution of copper and the cathodic reduction of the dissolved oxygen.

Impedance spectra of 4-MPP SAMs-modified copper changed significantly from that of unmodified copper. Semi-circles with much bigger diameters were observed in the case of 4-MPP SAMs-covered copper. Generally, the impedance of the 4-MPP SAMs-covered copper increased with increasing self-assembling time.

Many different equivalent circuits have been established to interpret impedance data of the SAMs-modified electrodes[6,7,22,23,24,25,2627]. The impedance data for SAMs-modified copper substrates were fit using the equivalent circuit described in chapter 4 for SAMs-modified gold substrates. The parameters values of the equivalent circuit elements obtained by fitting are given in Table 5.1. To evaluate the protective property of 4-MPP SAMs, the protection efficiency (PE) of SAMs was calculated using the equation 5.2:

$$PE(\%) = \frac{R_{sam} - R_t}{R_{sam}} \times 100 \qquad (5.2)$$

where R_{sam} is the transfer resistance of electrons through the 4-MPP monolayers and R_t is the charge-transfer resistance for the unmodified copper electrode in the corrosive solution. PE values of 4-MPP SAMs corresponding to different self-assembling time from the acetone solution were calculated and are also given in table 5.1. The PE values are found to increase with the self-assembling time. R_{sam} of 4-MPP SAMs formed from 30 minutes self-assembling was double of the charge transfer resistance of unmodified copper surface and had fair protection on copper surface. When the self-assembling time increased to 18 hours, R_{sam} increased from 32.4 KΩ (30 minutes self-assembling) to 69.4 KΩ, and 4-MPP SAMs provided a good protection on copper corrosion in NaCl solution.

Table 5.1. CNLS Fitting Parameters for 4-MPP SAMs-covered copper as a Function of Self-Assembling Time

Time(h)	$R_{sam}(10^4\Omega)$	CPE(μF)	α	PE (%)
0.5	3.24±0.02	47.27±0.25	0.623±0.003	53.4
1	3.50±0.03	46.25±0.27	0.624±0.004	57.3
12	4.66±0.02	33.18±0.13	0.640±0.003	67.5
18	6.94±0.05	26.06±0.13	0.693±0.004	78.1

To address the effect of molecular structure on the SAMs protection properties, impedance spectra were also obtained for 3-MPP SAMs prepared by immersing copper electrode in 2 mM 3-MPP acetone solution for 18 hours and compared with the data obtained with 4-MPP SAMs prepared using the same conditions. Values of R_{sam} and PE for 3- and 4-MPP SAMs are given in table 5.2. The coating resistance of 3-MPP SAMs was 2.5 times higher than that of 4-MPP SAMs; therefore, 3-MPP SAMs have higher protection efficiency and provide better protection against copper corrosion in NaCl solutions. Due to the difficulties in obtaining RAIR spectra and reductive desorption spectra on copper electrodes, the orientation of molecules on copper surface and the surface coverage of SAMs are not determined in our lab, and a thorough explanation of the different copper corrosion protection abilities between 3- and 4-MPP SAMs is not able to be given here. Considering the reported small tilt angle of SAMs on copper substrates and the different substitution patterns between 3- and 4-MPP molecules, the better corrosion protection of 3-MPP SAMs might be attributed to the higher covering area of 3-MPP molecules than 4-MPP molecules. Comparing to 4-MPP molecule in which imide groups are substituted at 4-position, 3-MPP

molecule with imide groups substituted at 3-position may cover more surface area and prevent the penetration of ions into SAMs more efficiently.

Table 5.2. Values of R_{sam} determined by fitting the impedance data to an equivalent circuit and the values of PE calculated for 3- and 4-MPP SAMs covered copper electrodes

SAM	$R_{sam}(10^4\Omega)$	PE (%)
3-MPP	18.11±2.64	91.6±19.8
4-MPP	6.94±0.85	78.1±15.5

5.2.2. Polarization Measurements

Polarization curves of unmodified and 4-MPP SAMs-modified copper electrodes in 0.2 M NaCl solutions are shown in Figure 5.3. The values of the exchange current densities for the cathodic and anodic reactions have a profound effect on the corrosion rate, i_{corr}. For the 4-MPP monolayer modified electrode, both anodic and cathodic currents were reduced compared to the unmodified copper electrode. This results in a lower corrosion current density on the SAMs-modified copper electrodes and indicated the retardant of the copper corrosion by the SAMs. It is also observed that the i_{corr} decreased and the corrosion protection of 4-MPP SAMs increased with the increasing self-assembling time of copper electrodes in 4-MPP acetone solution.

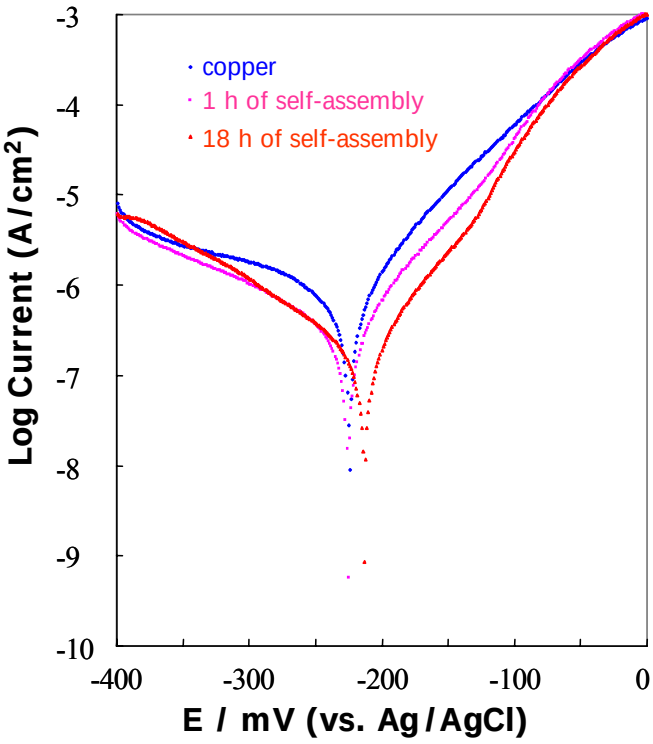

Figure 5.3. Anodic and cathodic Tafel lines for uncovered and 4-MPP SAMs-covered copper electrodes in 0.2 M NaCl solutions at the potential scan rate of 0.2 mV/s. The self-assembling time of copper electrodes in 2 mM 4-MPP acetone solutions are marked in the plots.

Values of the corrosion current density and protection efficiency (PE) of 4-MPP SAMs with various self-assembling time are given in Table 5.3. For these measurements, the PE is defined as:

$$PE(\%) = \frac{i_{corr} - i_{corr}'}{i_{corr}} \times 100 \qquad (5.3)$$

where i_{corr} and i'_{corr} are the corrosion current densities of the unmodified and 4-MPP SAMs modified copper electrodes, respectively, determined by the Tafel extrapolation method discussed previously. The corrosion current density, i_{corr}, decreased dramatically on 4-MPP SAMs-modified copper electrodes, indicating the corrosion protection of 4-MPP

SAMs on copper surfaces. By increasing the self-assembling time, the i_{corr} and the corrosion rate decreased, so the protection efficiency increased. These results revealed that the best protection was obtained using the longest self-assembling time. This is in good agreement with impedance spectroscopy results.

Table 5.3. Corrosion current densities of the uncovered and 4-MPP SAMs covered copper electrodes and protection efficiency (PE) of 4-MPP SAMs in NaCl solutions

Time(h)	0	1	12	18
i_{corr} (10^{-7}A/cm^2)	9.973	3.307	2.467	1.832
PE (%)	-	66.8	74.6	81.2

The copper corrosion protection action of 3- and 4-MPP SAMs prepared under the same conditions was also studied by polarization measurements. Values of the corrosion current density and protection efficiency (PE) are given in Table 5.4. Compared to 4-MPP SAMs, 3-MPP SAMs have lower corrosion current intensity and higher protection efficiency. Tafel plot results again suggested better copper corrosion protection of 3-MPP SAMs in NaCl solution, which is in agreement with electrochemical impedance spectroscopy results.

Table 5.4. Corrosion current densities and protection efficiency (PE) of 3- and 4-MPP SAMs covered copper electrodes in NaCl solutions

SAM	i_{corr} (10^{-7}A/cm2)	PE (%)
3-MPP	1.33±0.08	86.3±6.2
4-MPP	1.75±0.26	82.0±12.8

5.3 Conclusions

Copper corrosion protection behaviors of 3- and 4-MPP monolayers were investigated using impedance spectroscopy and polarization measurements. Both methods suggested that these aromatic thiol SAMs can protect copper from corrosion in NaCl solution, and better corrosion protection in NaCl solutions was obtained with longer self-assembling time. 3-MPP monolayers with imide groups substituted at 3-positions showed higher protection efficiency than 4-MPP monolayers probably because 3-MPP molecule covered more area on the copper surface and prevented ions penetration from solution to copper surface more efficiently. Spectroscopic, electrochemical, and other additional evidence are needed to get a better understanding on the mechanism of the copper corrosion protection of aromatic thiols SAMs.

5.4 References

1. Laibinis, P. E.; Whitesides, G. M.; Allara, D. L.; Tao, Y.-T.; Parikh, A. N.; Nuzzo, R. G. *J. Am. Chem. Soc.* **1991,** *113,* 7152

2. Laibinis, P. E.; Whitesides, G. M. *J. Am. Chem. Soc.* **1992,** *114,* 1990

3. Laibinis, P. E.; Whitesides, G. M. *J. Am. Chem. Soc.* **1992,** *114,* 9022

4. Jennings, G. K.; Laibinis, P. E. *Colloids Surf., A* **1996,** *116,* 105

5. Scherer, J.; Vogt, M. R.; Magnussen, O. M.; Behm, R. J. *Langmuir* **1997,** *13,* 7045

6. Feng, Y. Q.; Teo, W. K.; Siow, K. S.; Gao, Z. Q.; Tan, K. L.; Hsieh, A. K. *J. Electrochem. Soc.* **1997,** *144,* 55

7. Jennings, G. K.; Munro, J. C.; Yong, T. –H.; Laibinis, P. E. *Langmuir* **1998,** *14,* 6130

8. Ma, H. Y.; Yang, C.; Chen, S. H.; Jiao, Y. L.; Huang, S. X.; Li, D. G.; Luo, J. L. *Electrochimica Acta* **2003,** *48,* 4277

9. Yamamoto, Y.; Nishihara, H.; Aramaki, K. *J. Electrochem. Soc.* **1993,** *140,* 436

10. Itoh, M.; Nishihara, H.; Aramaki, K. *J. Electrochem. Soc.* **1994,** *141,* 2018

11. Haneda, R.; Nishihara, H.; Aramaki, K. *J. Electrochem. Soc.* **1997,** *144,* 1215

12. Haneda, R.; Nishihara, H.; Aramaki, K. *J. Electrochem. Soc.* **1998,** *145,* 1856

13. Haneda, R.; Aramaki, K. *J. Electrochem. Soc.* **1998,** *146,* 2786

14. Sinapi, F.; Delhalle, J.; Mekhalif, Z. *Materials Science and Engineering C* **2002,** *22,* 345

15. Lusk, A. T.; Jennings, G. K. *Langmuir* **2001,** *17,* 7830

16. Li, S. L.; Wang, Y. G.; Chen, S. H.; Yu, R.; Lei, S. B.; Ma, H. Y.; Liu D. X *Corrosion Science* **1999,** *41,* 1769

17. Quan, Z. L.; Chen, S. H.; Li, S. L *Corrosion Science* **2001,** *43,* 1071

18. Quan, Z. L.; Chen, S. H.; Li, Y.; Cui, X. G. *Corrosion Science* **2002,** *44,* 703

19. Ma, H.; Cheng, X.; Li, G.; Chen, S.; Quan, Z.; Zhao, S.; Niu, L. *Corros. Sci.* **2000,** *42,* 1669

20. Barcia, O. E.; Matoos, O. R.; Pebere, N.; Tribollet, B. *J. Electrochem. Soc.* **1993,** *140,* 2825

21. Barcia, O. E.; Matoos, O. R. *Electrochim. Acta* **1990,** *35,* 1601

22. Zamborini, F. P.; Crooks, R. M. *Langmuir* **1998,** *14,* 3279

23. Nahir, T. M.; Bowden, E. F. *Electrochim. Acta* **1994,** *39,* 2347

24. Boubour, E.; Lennox, R. B. *J. Phys. Chem. B* **2000,** *104,* 9004

25. Boubour, E.; Lennox, R. B. *Langmuir* **2000,** *16,* 7464

26. Janek, R. P.; Fawcett, W. R. *Langmuir* **1998,** *14,* 3011

27. Janek, R. P.; Fawcett, W. R. *J. Phys. Chem. B* **1997,** *101,* 8550

Chapter 6

Summary

The structure of molecules composing self-assembled monolayers affects the interfacial monolayer properties such as wetting, adhesion, and corrosion by changing intermolecular forces (van der Waals interactions, hydrogen bonding, π-π interactions), molecular substrate interactions, and molecule-solvent interactions. Understanding the fundamental relationships between structure and interfacial properties is critical to the potential applications of self-assembled monolayers.

3-aminothiophenol (3-ATP), 4-aminothiophenol (4-ATP), (3-mercaptophenyl) phthalimide (3-MPP), and (4-mercaptophenyl) phthalimide (4-MPP) molecules differ in either functional tail groups or substitution patterns on benzene ring. Self-assembled monolayers of ATP molecules have polar amine tail groups exposed to the outer surface, while monolayers of MPP molecules have non-polar imide tail groups exposed to the outer surface. Substitutions at 3-position have a 60 degree difference with substitutions at 4-position. These structural differences make it possible to study the influence of the microscopic structural on the macroscopic physical properties.

Self-assembled monolayers are applied as a coupling agent for improving adhesion in polymer/metal systems where the polymer has poor adhesion to the metal substrates. This can be achieved through surface reaction on self-assembled monolayers. Reaction of 3- and 4-ATP SAMs toward phthalic anhydride (PA) on the gold surfaces is investigated to understand the influence of molecular structure on the

monolayer reactions. Products of these monolayer reactions are 3-, and 4-MPP SAMs, respectively. The appearance of imide peaks and the decrease in the intensity of amine peaks in reflection absorption infrared spectroscopy, the absence of an obvious amine oxidation peak observed in cyclic voltammetry spectra on the reacted surface, and the change of SAM's thickness before and after the surface reaction demonstrated the covalent attachment of the anhydride. Results of the contact angle measurements of mixed two-component ATP and MPP SAMs and the reacted surface indicated that the reactivity of 3-ATP toward PA is a little bit higher than that of 4-ATP.

When self-assembled monolayers are in contact with an electrolyte solution, self-assembled monolayer/metal system can be modeled as a capacitor with current leakage at defect sites. Electrochemical impedance spectroscopy is used to study the ionic insulating properties of these four SAMs on gold surface by fitting the experimental data with an appropriate equivalent circuit. The appropriate measurement condition was determined to be 50 mM Na_2HPO_4 with 200 mV DC potential in the frequency range 10 KHz – 1 Hz. Impedance of 3-, and 4-ATP, 3- and 4-MPP SAMs determined under this condition indicated that 4-MPP SAMs had the highest monolayer resistance and showed the highest resistance to the ion transport among them. It was found that 4-MPP monolayer has the highest contact angle and most negative reductive desorption potential. These results indicated the hydrophobicity of the 4-MPP monolayer and the strong stabilizing lateral interactions within the 4-MPP monolayer. These might account to its passivating properties on gold substrates.

Copper is an important metal in the chemical and microelectronic industries; however, it is active and can be spontaneously oxidized on exposure to atmosphere. The development of coatings that provide the requisite protection of the copper surface is essential for its efficient use in these applications. Copper corrosion protection of 3- and 4-MPP monolayers was studied using electrochemical impedance spectroscopy and polarization measurements. Protection of copper in corrosive NaCl solution was observed for these aromatic thiol SAMs in both measurements. Both experiments indicated better corrosion protection with longer self-assembling time. Impedance of 3- and 4-MPP SAMs prepared under the same conditions was tested to analyze the influence of molecular structure on the copper corrosion protection. Higher protection efficiency was determined for 3-MPP monolayers than 4-MPP monolayer using these two methods. The reason might be the more surface area covered by 3-MPP due to the different substitution pattern on benzene ring and the better prevention of ion penetration from solution to copper surface.

Aromatic thiols of more benzene rings are the direction of future work. Monolayers composed of molecules with more benzene rings might have stronger interactions within monolayers and might be able to form more densely packed and ordered monolayers to provide better interfacial properties. Above results showed different ionic insulating properties for 3- and 4-MPP on the gold and copper substrates, another direction of future work can be spectroscopic and electrochemical studies on the self-assembled monolayers on copper surface to obtain a picture of the monolayer.

Vita

Huimin Li was born in Hongjiang, Hunan Province, People's Republic of China in 1969. After graduation from high school in 1987, Huimin attended Hunan University in Changsha, Hunan Province. She worked as a chemical engineer in Shuguang Electronic Group Limited Company, Changsha for three year after she got her Bachelor degree in analytical chemistry at Hunan University. Then she accepted a faculty position at Hunan University. In August 1999, Huimin joined professor Mark R. Anderson's group to pursue her Ph. D.